Supporting Information

Consecutive one-/two-step relaxation transformations of single-molecule magnet via coupling dinuclear dysprosium compounds with chloride bridges

Haiquan Tian,*[a] Bao-Lin Wang,*[b] Jing Lu,[a] Hou-Ting Liu,[a] Jianhui Su,[a] Dacheng Li[a] and Jianmin Dou*[a]

Experimental Section

Synthetic procedures

(*E*)-N'-(2-hyborxy-3-methoxybenzylidene)pyrazine-2-carbohydrazide (H_2opch)[1] and (*E*)-N'-(2-hydroxybenzylidene)pyrazine-2-carbohydrazide (H_2spch)[2] was prepared according to the methods reported in the literatures. All chemicals were of reagent grade and were used without any further purification.

Synthesis of 1, 2, 1a and the diluted sample

[Dy(opch)Cl(MeOH)]$_2$ (1): The solution of $DyCl_3 \cdot 6H_2O$ (75.4 mg, 0.20 mmol) and the H_2opch (54.0 mg, 0.20 mmol) in 20 mL CH_3OH was stirred with triethylamine (0.07 mL, 0.50 mmol) for 24h, the mixture was transferred to a 25 mL glass ware and sealed. The reaction mixture was heated at 60 °C under auto-generated pressure. Red single crystals, suitable for X-ray diffraction analysis, were formed after for one week as single-phase product. Yield: 50 mg, (46%, based on Dy). Elemental analysis (%) calcd for $C_{28}H_{28}Cl_2Dy_2N_8O_8$: C, 33.61, H, 2.82, N, 11.20: found C, 32.85, H, 2.63, N, 10.89. IR (KBr, cm^{-1}): 3459(m), 1603(vs), 1560(m), 1475(s), 1445(s), 1382(w), 1341(m), 1306(w), 1247(m), 1215(m), 1174(w), 1082(w), 1034(m), 924(w), 900(w), 860(w), 790(w), 750(m), 544(m), 436(w).

[Dy$_2$(opch)$_2$(μ-Cl)Cl(MeOH)$_2$]$_2$ (2): The solution of $DyCl_3 \cdot 6H_2O$ (132.0 mg, 0.35 mmol) and the H_2opch (54.0 mg, 0.20 mmol) in 20 mL CH_3OH was stirred with triethylamine (0.028 mL, 0.2 mmol). After 24h, H_2spch (48.4 mg, 0.20 mmol) was added to the solution. Then the mixture was stirred for anpther 48 h, and the resulting solution was transferred to a 25 mL glass ware and sealed. The reaction mixture was heated at 80 °C under auto-generated pressure. Deep brown single crystals, suitable for X-ray diffraction analysis, were formed after for 5 days as single-phase product. Yield:

43 mg, (31%, based on Dy). Elemental analysis (%) calcd for $C_{56}H_{56}Cl_4Dy_4N_{16}O_{16}$: C, 33.61, H, 2.82, N, 11.20: found C, 32.57, H, 3.02, N, 10.94. IR (KBr, cm^{-1}): 3406(m), 1616(vs), 1556(m), 1521(w), 1479(m), 1451(s), 1439(s), 1420(s), 1391(m), 1341(m), 1285(m), 1240(m), 1241(s), 1159(m), 1081(m), 1020(m), 958(w), 914(w), 861(w), 745(m), 685(w), 641(m), 586(w), 519(w), 455(w).

$[Dy(opch)Cl(MeOH)]_2$ (1a): This compound was prepared as red single crystals using a similar method to that of **2**, except that the reaction mixture was heated at 100 °C under auto-generated pressure. Yield: 33 mg, (24%, based on Dy). Elemental analysis (%) calcd for $C_{28}H_{28}Cl_2Dy_2N_8O_8$: C, 33.61, H, 2.82, N, 11.20: found C, 32.34, H, 2.98, N, 10.85. IR (KBr, cm^{-1}): 3464(m), 1602(vs), 1560(m), 1475(s), 1446(s), 1383(w), 1342(m), 1312(w), 1248(m), 1215(m), 1194(w), 1084(w), 1034(m), 956(w), 925(w), 860(w), 762(w), 752(m), 544(m), 436(w).

$[Dy_{0.1}Y_{0.9}(opch)Cl(MeOH)]_2$ (1-$Dy_{0.1}Y_{0.9}$): The site-substituted **1-$Dy_{0.1}Y_{0.9}$** sample was synthesized in accordance with the synthesis of pure **1** (see above), with an accurately measured 1:9 molar ratio of dysprosium(III) and yttrium(III) chloride starting materials.

$[Dy_{0.1}Y_{0.9}(opch)_2(\mu\text{-}Cl)Cl(MeOH)_2]_2$ (2-$Dy_{0.1}Y_{0.9}$): The site-substituted **2-$Dy_{0.1}Y_{0.9}$** sample was synthesized in accordance with the synthesis of pure **2** (see above), with an accurately measured 1:9 molar ratio of dysprosium(III) and yttrium(III) chloride starting materials.

$[Dy_{0.1}Y_{0.9}(opch)Cl(MeOH)]_2$ (1a-$Dy_{0.1}Y_{0.9}$): The site-substituted **1a-$Dy_{0.1}Y_{0.9}$** sample was synthesized in accordance with the synthesis of pure **1a** (see above), with an accurately measured 1:9 molar ratio of dysprosium(III) and yttrium(III) chloride starting materials.

Single-Crystal Structure Determination

Single crystals of dimensions 0.20 × 0.15 × 0.10 mm^3 for compound **1**, 0.15 × 0.10 × 0.08 mm^3 for compound **2** and 0.15 × 0.10 × 0.10 mm^3 for compound **1a** were mounted on a glass rod. The crystal data were collected on a Bruker SMART APEX II diffractometer using monochromated Mo-Kα radiation (λ = 0.71073 Å) at 293(2) K for compounds **1**, **2** and **1a**. The structures were solved by direct methods and refined on F^2 by full matrix least squares using SHELXTL.[3] All non-hydrogen atoms were refined anisotropically. All hydrogen atoms were either put in calculated positions or found from the difference Fourier maps and refined isotropically. Selected bond lengths and

angles are given in Table S2.

Physical measurements

Elemental analysis for C, H, and N was carried out on a Perkin-Elmer 2400 analyzer. FTIR spectra were recorded with a VERTEX 70 Fourier transform infrared spectrophotometer using the reflectance technique (4000–300 cm^{-1}). Samples were prepared as KBr disks. Magnetic susceptibility measurements were performed in the temperature range 1.9–300 K using a vibrating sample magnetometer (VSM) of Quantum Design MPMS SQUID-VSM system. The diamagnetic corrections for the compounds were estimated using Pascal's constants.[4]

References:

1. H. Tian, L. Zhao, Y.-N. Guo, Y. Guo, J. Tang and Z. Liu, *Chem. Commun*., 2012, **48**, 708-710.
2. H. Tian, Y.-N. Guo, L. Zhao, J. Tang and Z. Liu, *Inorg. Chem*., 2011, **50**, 8688-8690.
3. SHELXTL (version 5.0), Reference Manual, Siemens Industrial Automation, Analytical Instruments Madison, WI, 1995.
4. Olivier Kahn, *Molecular Magnetism*, VCH Publishers, Inc., New York, **1993**.

Table S1. Summary of structural data of **1**, **2** and **1a**.

Compound	**1**	**2**	**1a**
Formula	$C_{28}H_{28}Cl_2Dy_2N_8O_8$	$C_{56}H_{56}Cl_4Dy_4N_{16}O_{16}$	$C_{28}H_{28}Cl_2Dy_2N_8O_8$
M_r	1000.48	2000.97	1000.48
Cryst size	0.20 × 0.15 × 0.10	0.15 × 0.10 × 0.08	0.15× 0.10 × 0.10
T [K]	293(2)	293(2)	293(2)
λ [Å]	0.71073	0.71073	0.71073
crystal syst	triclinic	monoclinic	triclinic
space group	*P*-1 #2	*P*21/*c* #14	*P*-1 #2
a [Å]	9.159(9)	9.416(4)	9.292(4)
b [Å]	9.343(11)	21.374(8)	9.345(3)
c [Å]	11.151(13)	16.637(7)	21.486(9)
α [deg]	88.62(5)	90	80.320(14)
β [deg]	73.41(4)	104.907(8)	80.796(12)
γ [deg]	67.12(3)	90	65.327(11)
V [Å^3]	838.5(16)	3236(2)	1662.8(11)
Z	1	2	2
ρ[g cm^{-3}]	1.981	2.054	1.998
2θ [deg]	2.4 – 25.0	2.9 – 25.0	2.5 – 25.0
R_{int}	0.068	0.057	0.047
GOF	1.05	1.25	1.15
$R1$ [$I > 2\sigma(I)$], w$R2$ (all data)	0.0521, 0.1301	0.0409, 0.0715	0.0509, 0.1274
$(\Delta\rho)_{max}$, $(\Delta\rho)_{min}$/[e Å^{-3}]	0.44, -0.33	0.80, -0.81	1.59, -1.80
CCDC number	1862369	1862368	1862367

Table S2. Selected bond lengths (Å) and angles (º) for compounds **1**, **2** and **1a**.

Compound 1					
Dy1–O1	2.328(7)	Dy1–Cl1	2.593(4)	Cl1–Dy1–N4	96.5(2)
Dy1–O2	2.137(7)	Dy1···Dy1A	3.851(4)	Cl1–Dy1–N1A	132.7(2)
Dy1–O4	2.584(2)	Cl1–Dy1–O1	93.6(2)	Cl1–Dy1–N1A	170.3(1)
Dy1–O1A	2.324(6)	Cl1–Dy1–O2	101.6(2)	Dy1–O1–Dy1A	111.8(3)
Dy1–N4	2.451(9)	Cl1–Dy1–O4	170.3(2)		
Dy1–N1A	2.571(9)	Cl1–Dy1–O1A	90.1(2)		
Symmetry code: A: 2-x,1-y,1-z.					
Compound 2					
Dy1–O2	2.129(5)	Dy1–Cl2	2.774(2)	Cl2–Dy2–O8	148.3(2)
Dy1–O3	2.303(3)	Dy2–Cl2a	2.851(2)	Cl2–Dy2–N3	121.3(2)
Dy2–O6	2.293(4)	Dy1···Dy2	3.886(1)	Cl2–Dy2–N5	87.6(1)
Dy2–O7	2.341(5)	Dy2···Dy2A	4.630(1)	Cl2–Dy2–O3	85.3(2)
Dy1–N1	2.409(5)	Cl1–Dy1–O2	100.3(2)	Cl2–Dy2–Cl2A	69.2(1)
Dy1–N8	2.492(5)	Cl1–Dy1–O3	89.6(2)	Cl2A–Dy2–O3	105.9(1)
Dy1–Cl1	2.658(2)	Cl1–Dy1–O6	86.2(2)	Cl2A–Dy2–O5	76.7(2)
Dy2–O3	2.371(4)	Cl1–Dy1–O7	170.3(2)	Cl2A–Dy2–O6	142.9(2)
Dy2–O5	2.157(5)	Cl1–Dy1–N1	90.1(1)	Cl2A–Dy2–N3	73.2(2)
Dy2–O6	2.345(4)	Cl1–Dy1–N8	93.5(2)	Cl2A–Dy2–N8	118.2(2)
Dy2–O8	2.384(5)	Cl2–Dy2–O3	85.3(2)	Dy1–Cl2–Dy2A	110.8(2)
Dy2–N3	2.566(5)	Cl2–Dy2–O5	125.7(2)	Dy1–O3–Dy2	112.5(2)
Dy2–N5	2.483(5)	Cl2–Dy2–O6	74.0(2)	Dy1–O6–Dy2	113.8(2)
Symmetry code: A: 1-x,1-y,1-z.					
Compound 1a					
Dy1–O1	2.310(7)	Dy2–O4B	2.367(6)	Cl1–Dy1–O1A	92.4(2)
Dy1–O2	2.161(6)	Dy2–N8	2.462(8)	Cl1–Dy1–N1A	93.3(2)
Dy1–O7	2.396(7)	Dy2–N6B	2.575(8)	Cl2–Dy2–O4	93.0(2)
Dy1–O1A	2.483(6)	Dy2–Cl2	2.593(3)	Cl2–Dy2–O5	102.0(2)
Dy1–N4	2.475(9)	Dy1···Dy1A	3.885(1)	Cl2–Dy2–O8	167.3(2)
Dy1–N1A	2.588(8)	Dy2···Dy2A	3.897(1)	Cl2–Dy2–O4B	89.3(2)
Dy1–Cl1	2.596(3)	Cl1–Dy1–O1	92.4(2)	Cl2–Dy2–N8	98.8(2)
Dy2–O4	2.327(7)	Cl1–Dy1–O2	99.7(2)	Cl2–Dy2–N6B	89.2(2)
Dy2–O5	2.152(6)	Cl1–Dy1–O7	172.8(2)	Dy1–O3–Dy1A	113.1(3)
Dy2–O8	2.386(7)	Cl1–Dy1–N4	94.2(2)	Dy2–O4–Dy2A	112.3(3)
Symmetry code: A: 1-x,1-y,1-z; B:1-x, 1-y, -z.					

Table S3. Dy^{III} geometry analysis of **1**, **2** and **2a** by SHAPE 2.1 software.

Compound 1		**Compound 1a**		
Geometry (CN = 7)	**Dy1**	**Geometry (CN = 7)**	**Dy1**	**Dy2**
HP-7	33.434	**HP-7**	33.829	32.717
HPY-7	23.907	**HPY-7**	24.217	23.347
PBPY-7	1.373	**PBPY-7**	1.197	1.360
COC-7	7.907	**COC-7**	8.377	7.845
CTPR-7	6.587	**CTPR-7**	6.762	6.552
JPBPY-7	5.934	**JPBPY-7**	5.727	5.772
JETPY-7	22.559	**JETPY-7**	23.200	22.663

Compound 2					
Geometry (CN = 7)	**Dy1**	**Geometry (CN = 8)**	**Dy2**	**Geometry (CN = 8)**	**Dy2**
HP-7	32.684	**OP-8**	34.829	**JETBPY-8**	27.038
HPY-7	24.397	**HPY-8**	23.279	**JBTPR-8**	4.047
PBPY-7	1.035	**HBPY-8**	12.522	**BTPR-8**	2.833
COC-7	7.144	**CU-8**	9.501	**JSD-8**	6.285
CTPR-7	5.919	**SAPR-8**	5.374	**TT-8**	10.295
JPBPY-7	5.865	**TDD-8**	3.055	**ETBPY-8**	22.464
JETPY-7	23.371	**JGBF-8**	10.422		

Lable	**Shape**	**Lable**	**Shape**
HP-7	Heptagon	CU-8	Cube (O_h)
HPY-7	Hexagonal pyramid (C_{6v})	SAPR-8	Square antiprism (D_{4d})
PBPY-7	Pentagonal bipyramid (D_{5h})	TDD-8	Triangular dodecahedron (D_{2d})
COC-7	Capped octahedron (C_{3v})	JGBF-8	Johnson gyrobifastigium J26 (D_{2d})
CTPR-7	Capped trigonal prism (C_{2v})	JETBPY-8	Johnson elongated triangular bipyramid J14 (D_{3h})
JPBPY-7	Johnson pentagonal bipyramid J13 (D_{5h})	JBTPR-8	Biaugmented trigonal prism J50 (C_{2v})
JETPY-7	Elongated triangular pyramid J7 (C_{3v})	BTPR-8	Biaugmented trigonal prism (C_{2v})
OP-8	Octagon	JSD-8	Snub diphenoid J84 (D_{2d})
HPY-8	Heptagonal pyramid (C_{7v})	TT-8	Triakis tetrahedron (T_d)
HBPY-8	Hexagonal bipyramid (D_{6h})	ETBPY-8	Elongated trigonal bipyramid (D_{3h})

Table S4. Relaxation fitting parameters from least-squares fitting of $\chi(\omega)$ data for compound **1**.

T	χ_T	χ_s	α	$\ln(\tau$ / s)
1.9	49.40	8.26	0.200	-2.376
2.2	44.36	8.15	0.186	-2.546
2.5	40.05	8.03	0.173	-2.652
3.0	35.20	7.84	0.157	-2.788
3.5	31.42	7.70	0.145	-2.880
4.0	28.41	7.59	0.132	-2.970
4.5	25.51	7.49	0.125	-3.073
5.0	22.81	7.19	0.112	-3.128
6.0	19.16	6.84	0.089	-3.209
7.0	16.09	5.91	0.075	-3.286
8.0	12.82	4.17	0.066	-3.349
9.0	10.28	2.72	0.060	-3.401
10.0	7.84	1.16	0.055	-3.496
11.0	5.90	-0.10	0.054	-3.638
12.0	4.17	-1.27	0.052	-3.765
13.0	3.24	-1.74	0.050	-3.952
14.0	2.29	-2.29	0.048	-4.142
15.0	1.12	-3.12	0.046	-4.336
16.0	0.43	-3.53	0.044	-4.639
17.0	-0.11	-3.79	0.037	-4.975
18.0	-0.39	-3.81	0.033	-5.275
19.0	-0.56	-3.84	0.028	-5.614
20.0	-0.83	-3.87	0.025	-5.856
21.0	-1.02	-3.98	0.022	-6.300
22.0	-1.34	-4.02	0.019	-6.651
23.0	-1.43	-4.07	0.016	-7.163
24.0	-2.77	-4.72	0.011	-7.537
25.0	-3.78	-5.97	0.010	-7.909
26.0	-4.51	-6.52	0.009	-8.257
27.0	-6.44	-7.61	0.008	-8.593
28.0	-7.82	-8.14	0.006	-8.959
29.0	-8.93	-9.28	0.005	-9.166

Table S5. Relaxation fitting parameters from least-squares fitting of $\chi(\omega)$ data for compound **2**.

		FR			SR		
T	$\chi_{s,\,tot}$	$\Delta\chi_1$	α_1	$\ln(\tau_1$ / s)	$\Delta\chi_2$	α_2	$\ln(\tau_2$ / s)
1.9	-2.231	85.45	0.775	-6.999	-67.07	0.769	-2.488
2.2	-2.142	77.04	0.713	-7.001	-59.99	0.710	-2.580
2.5	-2.027	68.97	0.692	-7.111	-59.15	0.708	-2.663
3.0	-1.983	61.62	0.659	-7.246	-53.72	0.703	-2.792
3.5	-1.816	52.29	0.596	-7.373	-47.01	0.658	-2.908
4.0	-1.762	43.03	0.533	-7.483	-42.77	0.596	-3.028
4.5	-1.627	35.86	0.475	-7.599	-38.36	0.532	-3.138
5.0	-1.565	28.44	0.437	-7.689	-32.54	0.474	-3.271
6.0	-1.406	22.53	0.400	-7.939	-27.00	0.436	-3.570
7.0	-1.308	16.65	0.391	-8.174	-23.80	0.399	-3.941
8.0	-1.239	9.12	0.381	-8.463	19.23	0.389	-4.352
9.0	-1.194	4.84	0.376	-8.755	-15.51	0.379	-4.789
10.0	-1.042	1.26	0.362	-9.091	-11.35	0.374	-5.246
11.0	-0.922	0.36	0.358	-9.461	-7.35	0.369	-5.705
12.0	-0.832	-0.52	0.341	-9.751	-4.16	0.366	-6.142
13.0	-0.726	-1.49	0.327	-10.038	-2.52	0.357	-6.546
14.0	-0.633	-3.83	0.314	-10.398	-1.14	0.351	-6.981
15.0	-0.568	-5.72	0.305	-10.715	-0.79	0.338	-7.333
16.0	-0.439	-7.64	0.293	-10.961	0.29	0.326	-7.608
17.0	-0.302	-9.94	0.282	-11.250	1.24	0.320	-7.868
18.0	-0.257	-11.26	0.267	-11.474	3.69	0.313	-8.070
19.0	-0.186	-13.51	0.251	-11.696	5.18	0.295	-8.245
20.0	-0.078	-15.37	0.240	-11.862	7.02	0.282	-8.397
21.0	0.192	-17.92	0.236	-12.026	9.89	0.271	-8.568
22.0	0.807	-19.85	0.232	-12.141	12.57	0.266	-8.687
23.0	1.965	-21.44	0.297	-12.276	15.33	0.253	-8.817

Table S6. Relaxation fitting parameters from least-squares fitting of $\chi(\omega)$ data for compound **1a**.

T	χ_T	χ_S	α	$\ln(\tau$ / s)
1.9	42.97	8.02	0.240	-4.246
2.2	38.46	5.53	0.236	-4.257
2.5	34.23	4.16	0.231	-4.261
3.0	30.67	2.76	0.228	-4.289
3.5	26.36	1.33	0.223	-4.303
4.0	22.71	0.14	0.219	-4.315
4.5	18.52	-0.32	0.215	-4.341
5.0	14.27	-0.53	0.211	-4.345
6.0	10.17	-0.67	0.207	-4.355
7.0	6.03	-0.87	0.202	-4.386
8.0	3.04	-0.94	0.196	-4.435
9.0	1.21	-0.95	0.190	-4.491
10.0	0.31	-0.98	0.186	-4.542
11.0	-0.39	-0.99	0.183	-4.674
12.0	-0.47	-1.00	0.179	4.859
13.0	-0.54	-1.02	0.175	-5.015
14.0	-0.57	-1.05	0.168	-5.199
15.0	-0.63	-1.06	0.163	-5.377
16.0	-0.69	-1.08	0.157	-5.573
17.0	-0.70	-1.11	0.152	-5.794
18.0	-0.77	-1.14	0.146	-5.991
19.0	-0.82	-1.17	0.141	-6.258
20.0	-0.88	-1.21	0.135	-6.446
21.0	-0.94	-1.25	0.132	-6.656
22.0	-1.01	-1.29	0.128	-6.869
23.0	-1.06	-1.33	0.123	-7.207
24.0	-1.12	-1.38	0.119	-7.534
25.0	-1.15	-1.40	0.112	-7.831
26.0	-1.17	-1.42	0.108	-8.114
27.0	-1.24	-1.45	0.079	-8.377
28.0	-1.29	-1.51	0.060	-8.598
29.0	-1.39	-1.69	0.048	-8.813
30.0	-1.50	-1.73	0.031	-9.042

Table S7. Relaxation fitting parameters from least-squares fitting of $\chi(\omega)$ data for the diluted ($Dy_{0.1}Y_{0.9}$) sample of **1**.

T	χ_T	χ_s	α	$\ln(\tau$ / s)
1.9	30.26	17.74	0.215	-1.356
2.2	27.17	16.83	0.208	-1.459
2.5	24.44	15.56	0.203	-1.607
3.0	21.31	13.69	0.199	-1.691
3.5	18.37	11.63	0.195	-1.812
4.0	15.50	9.49	0.191	-1.927
4.5	12.71	7.29	0.186	-2.131
5.0	10.50	5.50	0.182	-2.246
6.0	7.80	3.20	0.177	-2.365
7.0	5.65	1.35	0.173	-2.483
8.0	4.04	-0.04	0.169	-2.614
9.0	2.96	-0.96	0.165	-2.702
10.0	1.35	-2.35	0.161	-2.921
11.0	-0.23	-3.67	0.157	-3.154
12.0	-0.86	-4.14	0.150	-3.391
13.0	-2.48	-5.52	0.146	-3.639
14.0	-3.57	-6.43	0.142	-3.889
15.0	-4.15	-6.85	0.138	-4.138
16.0	-5.73	-8.27	0.133	-4.380
17.0	-7.31	-9.68	0.129	-4.629
18.0	-8.87	-11.12	0.126	-4.889
19.0	-9.95	-12.05	0.122	-5.164
20.0	-11.01	-12.99	0.117	-5.391
21.0	-12.11	-13.88	0.112	-5.780
22.0	-12.71	-14.29	0.087	-6.120
23.0	-13.27	-14.73	0.073	-6.578
24.0	-13.84	-15.16	0.064	-6.932
25.0	-14.90	-16.10	0.059	-7.258
26.0	-15.45	-16.55	0.054	-7.564
27.0	-16.50	-17.50	0.043	-7.848
28.0	-17.54	-18.46	0.026	-8.112
29.0	-18.56	-19.43	0.024	-8.363
30.0	-19.13	-20.88	0.021	-8.592
31.0	-20.84	-22.16	0.018	-8.815
32.0	-21.46	-23.54	0.016	-9.041
33.0	-22.37	-24.93	0.013	-9.256
34.0	-23.96	-26.04	0.012	-9.431
35.0	-24.72	-27.28	0.010	-9.623

Table S8. Relaxation fitting parameters from least-squares fitting of $\chi(\omega)$ data for the diluted ($Dy_{0.1}Y_{0.9}$) sample of **2**.

		FR			SR		
T	$\chi_{s,\,tot}$	$\Delta\chi_1$	α_1	$\ln(\tau_1$ / s)	$\Delta\chi_2$	α_2	$\ln(\tau_2$ / s)
1.9	-1.422	73.96	0.434	-3.788	-58.43	0.401	-2.570
2.2	-1.337	69.62	0.422	-3.866	-55.41	0.389	-2.664
2.5	-1.202	57.17	0.418	-3.904	-44.90	0.382	-2.691
3.0	-1.115	51.03	0.414	-3.989	-40.48	0.375	-2.790
3.5	-1.021	44.64	0.409	-4.025	-35.32	0.369	-2.830
4.0	-0.896	39.16	0.405	-4.060	-30.77	0.364	-2.861
4.5	-0.684	33.76	0.402	-4.105	-26.16	0.360	-2.897
5.0	-0.523	29.00	0.398	-4.137	-22.01	0.357	-2.913
6.0	-0.407	25.72	0.394	-4.171	-19.27	0.352	-2.939
7.0	-0.260	21.05	0.390	-4.197	-14.99	0.348	-2.942
8.0	-0.102	17.86	0.385	-4.230	-12.16	0.344	-2.959
9.0	0.369	14.78	0.381	-4.280	-0.08	0.339	-2.977
10.0	0.553	12.13	0.377	-4.346	-0.07	0.335	-2.990
11.0	0.706	8.39	0.372	-4.458	-0.06	0.331	-3.094
12.0	0.920	5.75	0.369	-4.636	-0.05	0.326	-3.195
13.0	1.133	4.93	0.366	-4.852	-0.04	0.322	-3.292
14.0	1.392	4.49	0.363	-5.082	-0.03	0.318	-3.391
15.0	1.676	4.12	0.358	-5.298	-0.02	0.313	-3.541
16.0	1.942	3.80	0.355	-5.454	-0.01	0.307	-3.698
17.0	2.218	3.53	0.351	-5.640	0.07	0.302	-3.886
18.0	2.443	3.39	0.348	-5.892	0.08	0.299	-4.018
19.0	2.671	3.00	0.343	-6.182	0.13	0.294	-4.161
20.0	2.915	2.72	0.339	-6.370	0.17	0.288	-4.292
21.0	3.241	2.42	0.336	-6.631	0.50	0.285	-4.399

Table S9. Relaxation fitting parameters from least-squares fitting of $\chi(\omega)$ data for the diluted ($Dy_{0.1}Y_{0.9}$) sample of **1a**.

T	χ_T	χ_s	α	$\ln(\tau$ / s)
1.9	55.40	0.60	0.191	-1.660
2.2	48.36	2.64	0.186	-1.690
2.5	43.80	5.20	0.173	-1.730
3.0	38.70	8.30	0.157	-1.801
3.5	34.92	10.08	0.145	-1.910
4.0	31.41	10.59	0.132	-2.102
4.5	28.51	10.49	0.125	-2.282
5.0	25.81	10.19	0.112	-2.501
6.0	22.16	9.84	0.090	-2.964
7.0	18.60	8.41	0.075	-3.472
8.0	15.33	6.67	0.066	-3.991
9.0	13.28	5.72	0.063	-4.504
10.0	10.84	4.16	0.060	-4.996
11.0	8.00	2.00	0.055	-5.466
12.0	6.22	0.78	0.051	-5.893
13.0	4.49	-0.50	0.049	-6.303
14.0	2.29	-2.32	0.046	-6.693
15.0	1.12	-3.76	0.042	-7.054
16.0	-1.02	-4.98	0.040	-7.419
17.0	-2.16	-5.84	0.038	-7.740
18.0	-2.79	-6.21	0.036	-8.071
19.0	-3.86	-7.14	0.033	-8.396
20.0	-4.48	-7.52	0.031	-8.660
21.0	-5.02	-7.98	0.030	-8.966
22.0	-6.02	-8.98	0.029	-9.110
23.0	-7.24	-9.76	0.027	-9.690
24.0	-7.68	-10.32	0.026	-9.754
25.0	-8.52	-10.48	0.024	-9.830
26.0	-8.98	-11.02	0.021	-9.923
27.0	-9.93	-12.07	0.018	-10.017
28.0	-11.50	-12.50	0.015	-10.129
29.0	-11.82	-13.18	0.014	-10.258
30.0	-12.56	-13.44	0.012	-10.367
31.0	-13.18	-14.03	0.011	-10.492

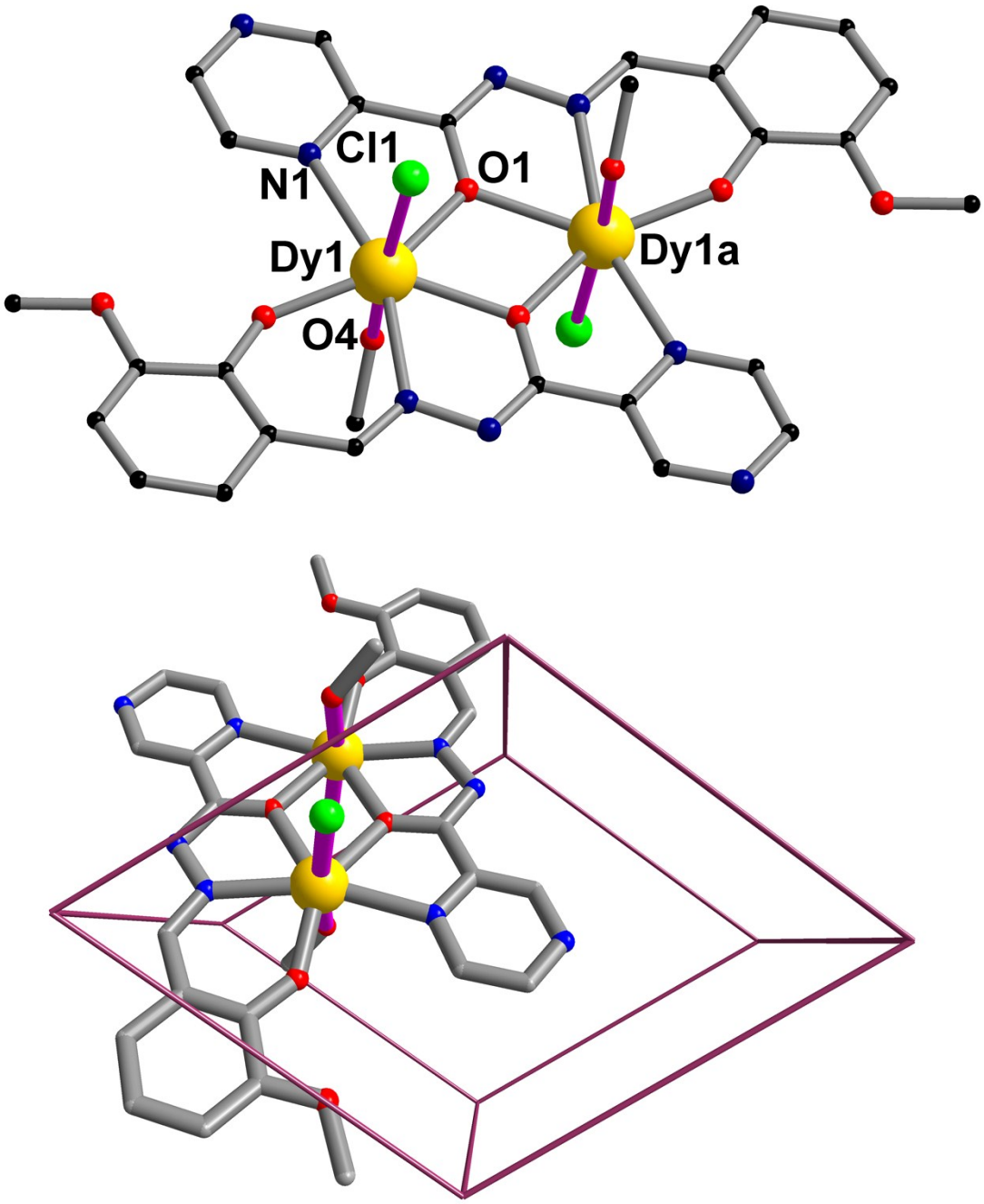

Figure S1. The molecular structures of compound **1** (top). Unit cell of **1** showing the presence of a isolated dinuclear molecule (bottom). Color scheme: Gold Dy, Bright green Cl, red O, blue N, black, C.

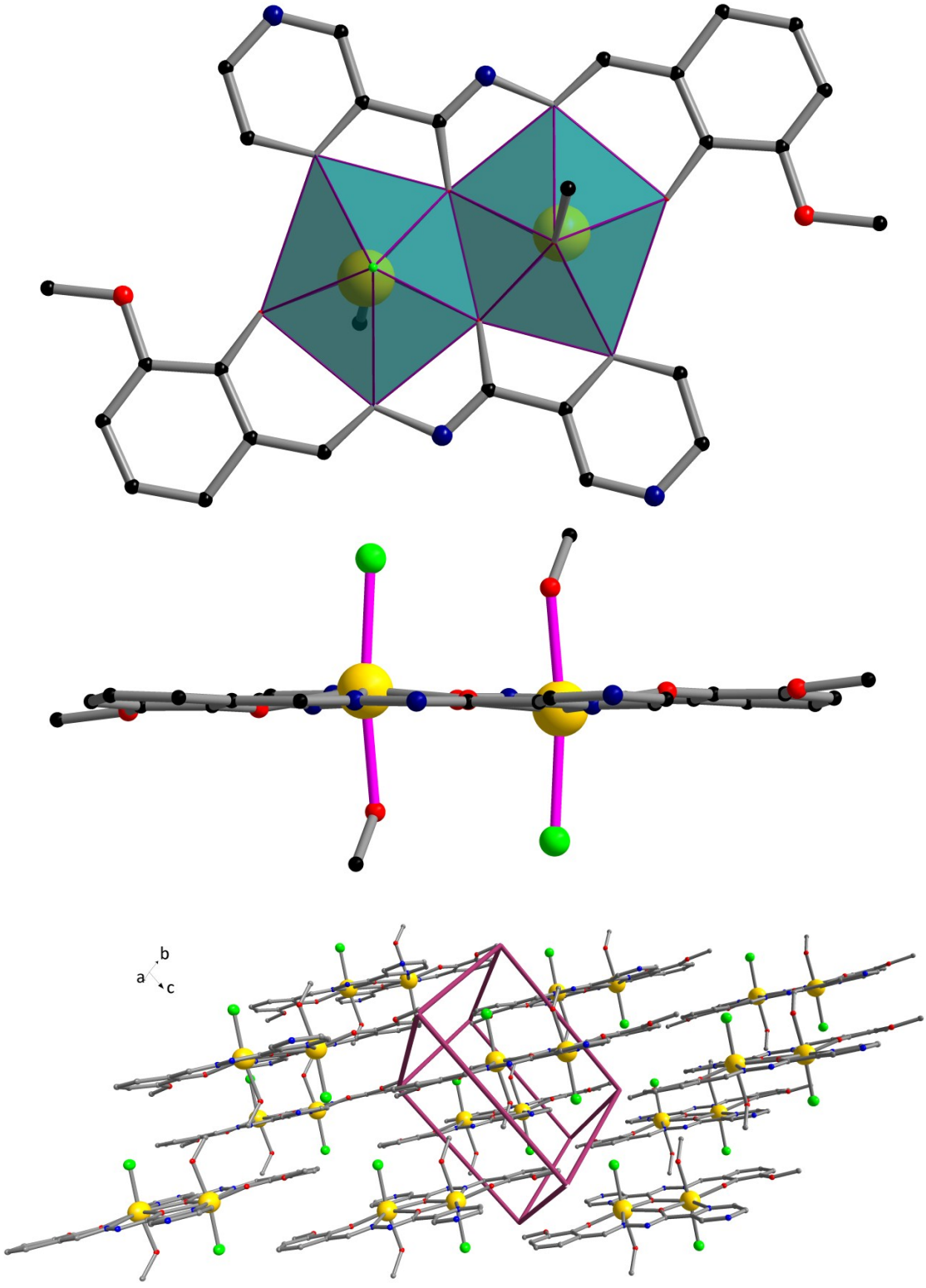

Figure S2. Coordination polyhedra observed of compound **1** (top). Side-view of the molecular structure (middle). Crystal packing of dinuclear unit showing a strictly co-parallel arrangement along the crystallographic different axes (bottom). Color scheme: Gold Dy, Bright green Cl, red O, blue N, black, C.

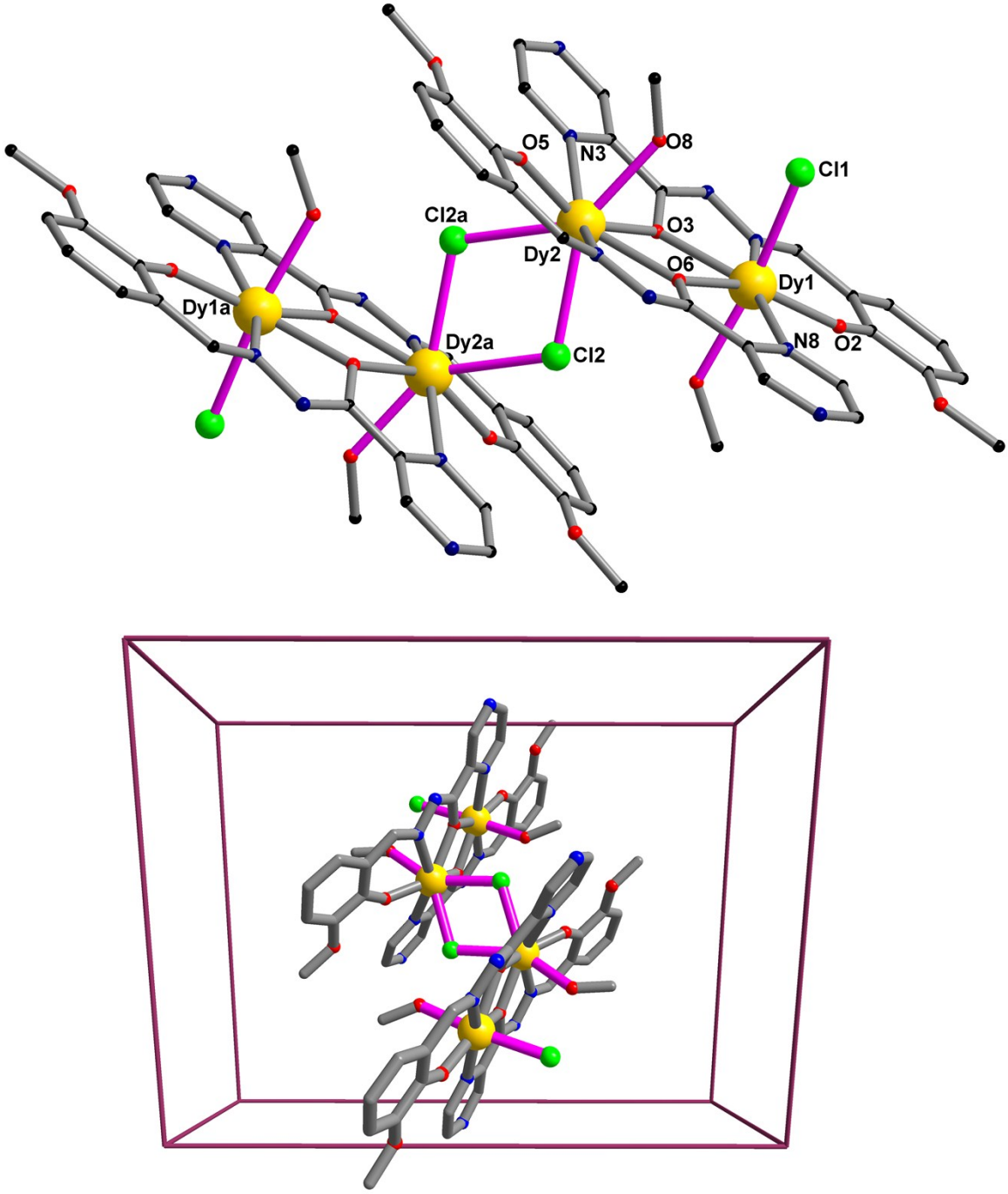

Figure S3. The molecular structures of compound **2** (top). Unit cell of **2** showing the presence of a double Cl-bridged dimer of dinuclear molecule (bottom). Color scheme: Gold Dy, Bright green Cl, red O, blue N, black, C.

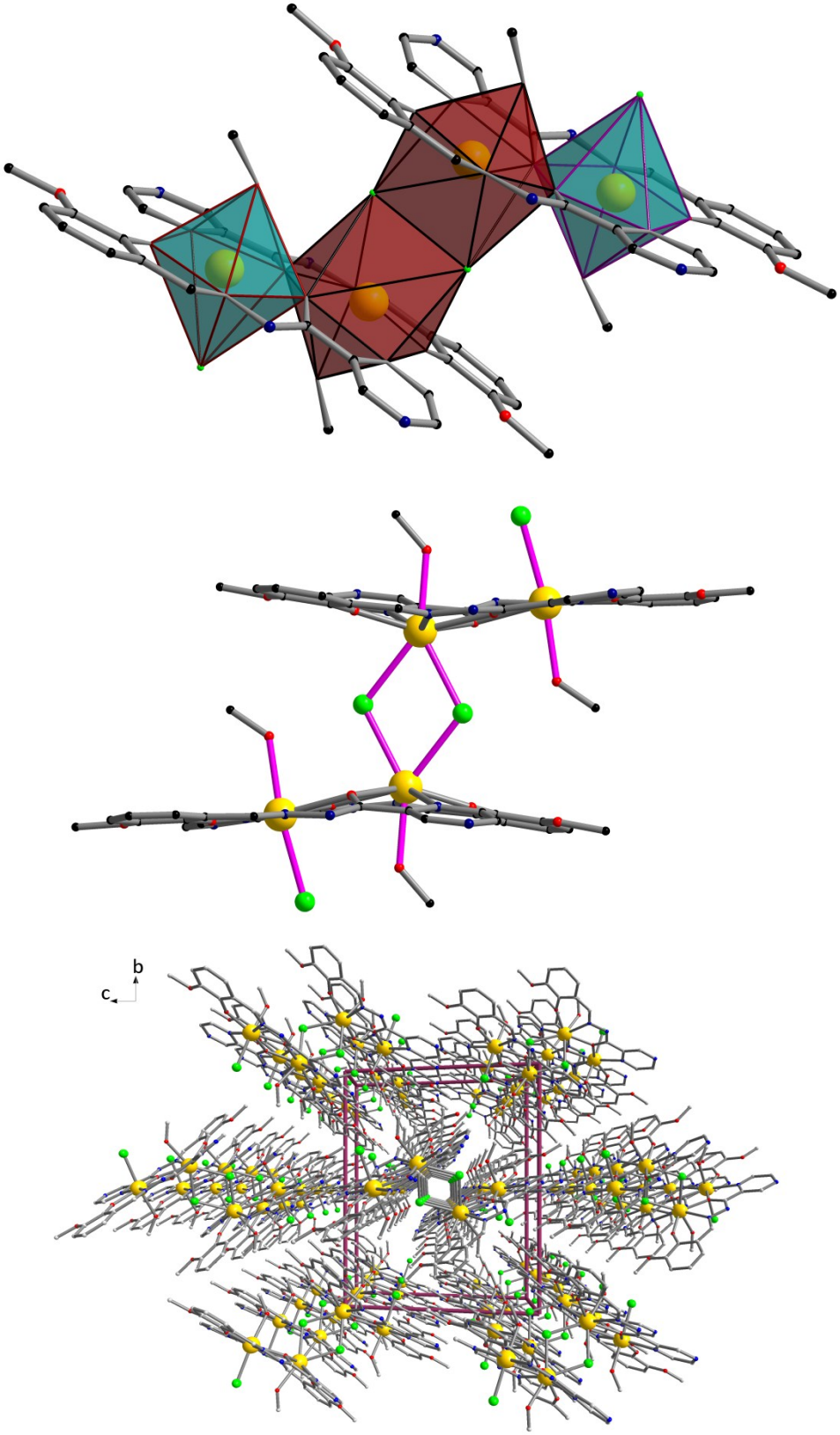

Figure S4. Coordination polyhedra observed of compound **2** (top). Side-view of the molecular structure (middle). Packing arrangement of tetranuclear unit along the crystallographic *a* axis (bottom). Color scheme: Gold Dy, Bright green Cl, red O, blue N, black, C.

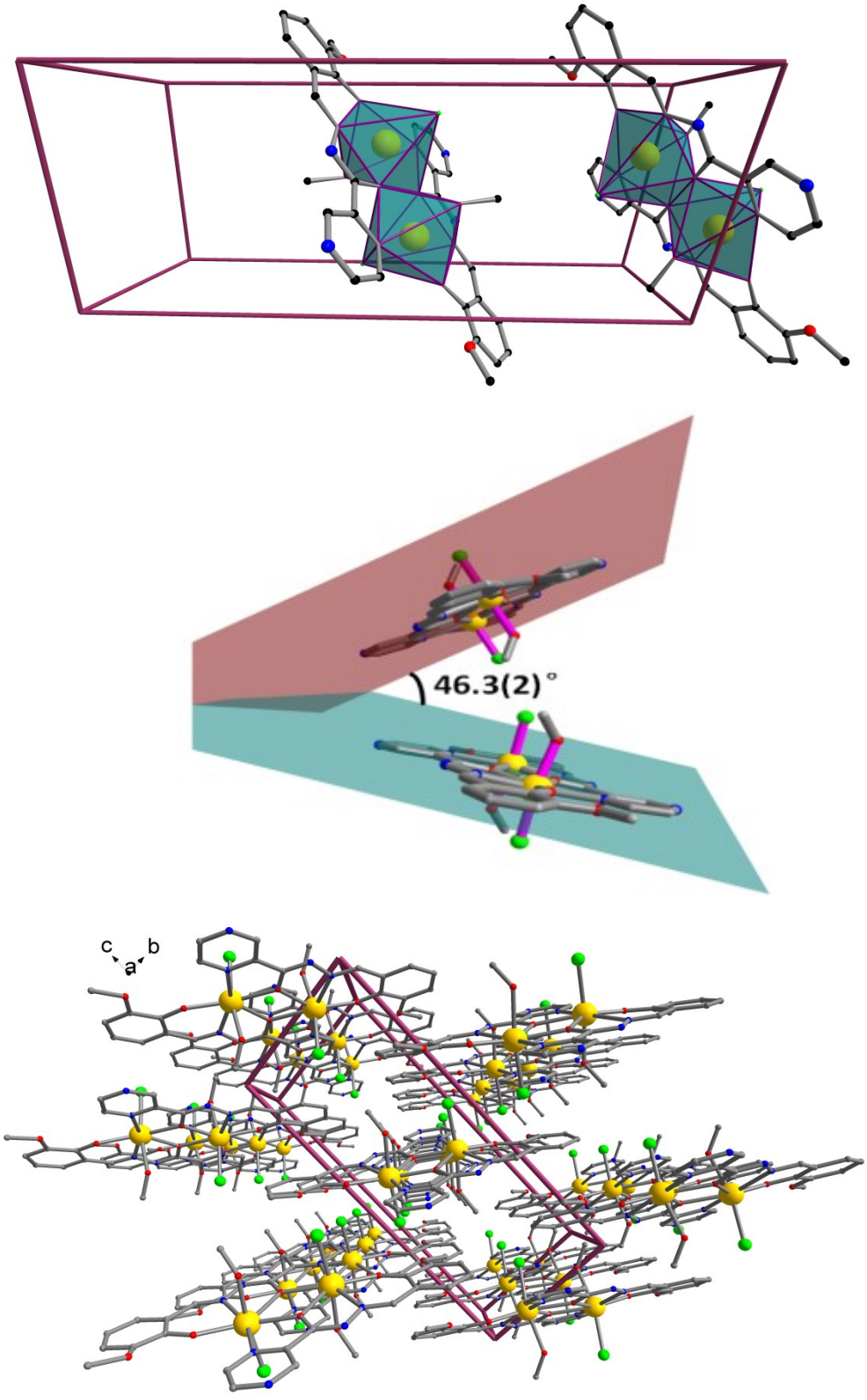

Figure S5. Coordination polyhedra observed of compound **1a** in the unit cell (top). The dihedral angle of the dinuclear building blocks for compound **1a** (middle). Packing arrangement of tetranuclear unit along the crystallographic *a* axis (bottom). Color scheme: Gold Dy, Bright green Cl, red O, blue N, black, C.

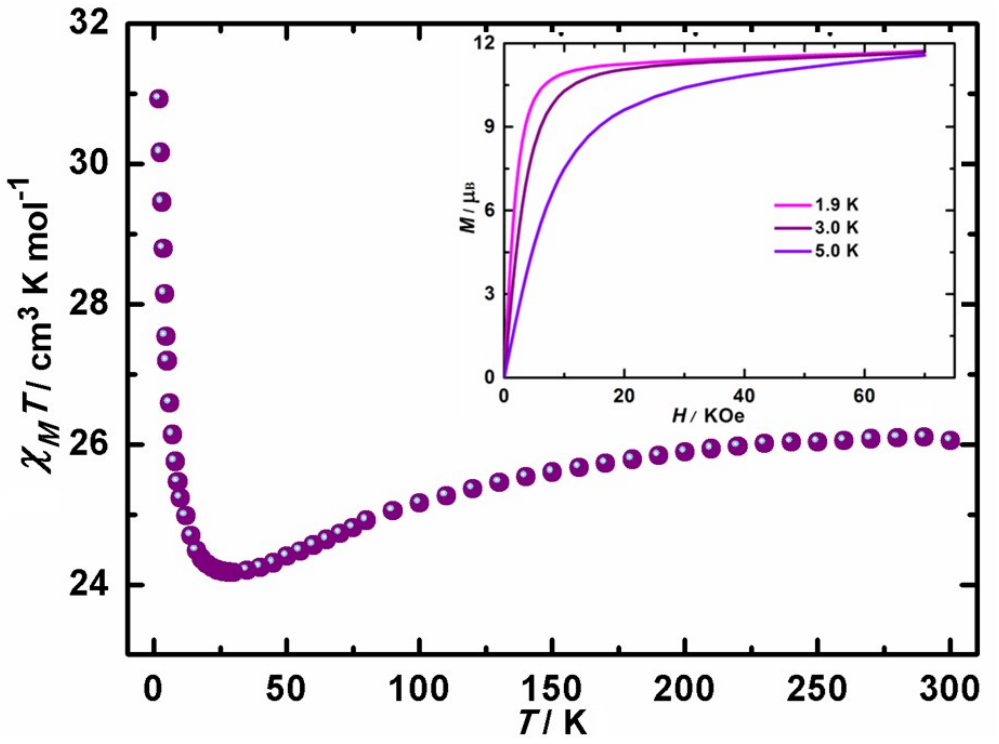

Figure S6. Temperature dependence of the $\chi_M T$ product at 1 kOe for **1**; inset: *M vs. H/T* plot at different temperatures below 5 K.

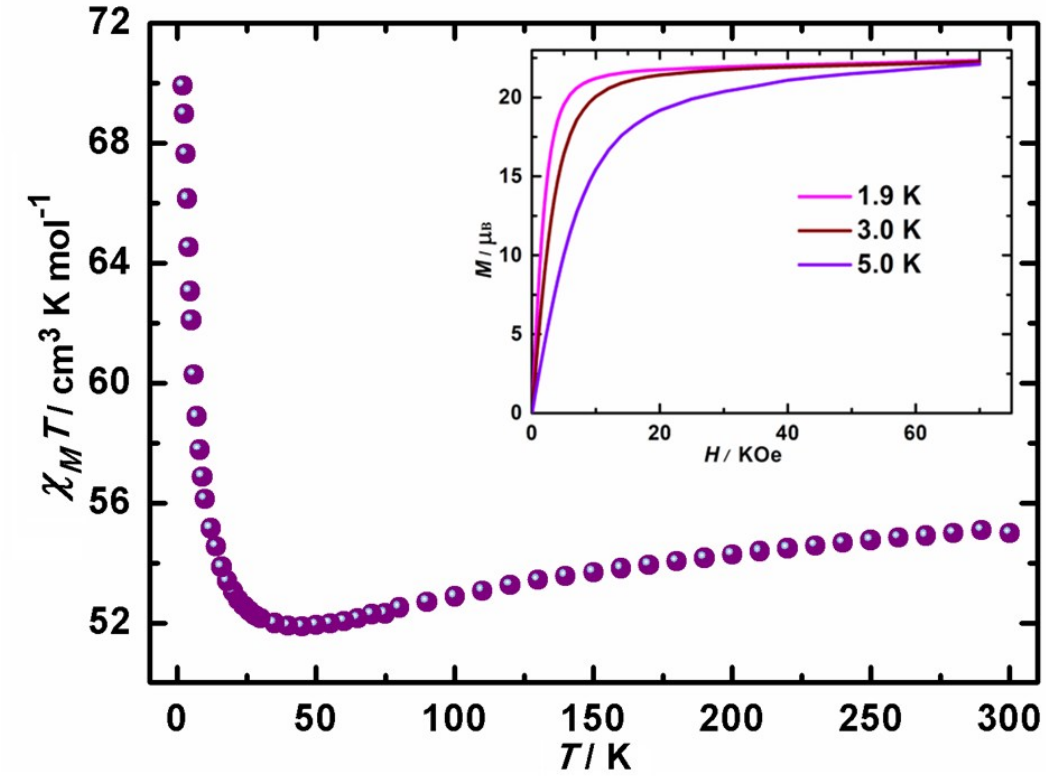

Figure S7. Temperature dependence of the $\chi_M T$ product at 1 kOe for **2**; inset: *M vs. H/T* plot at different temperatures below 5 K.

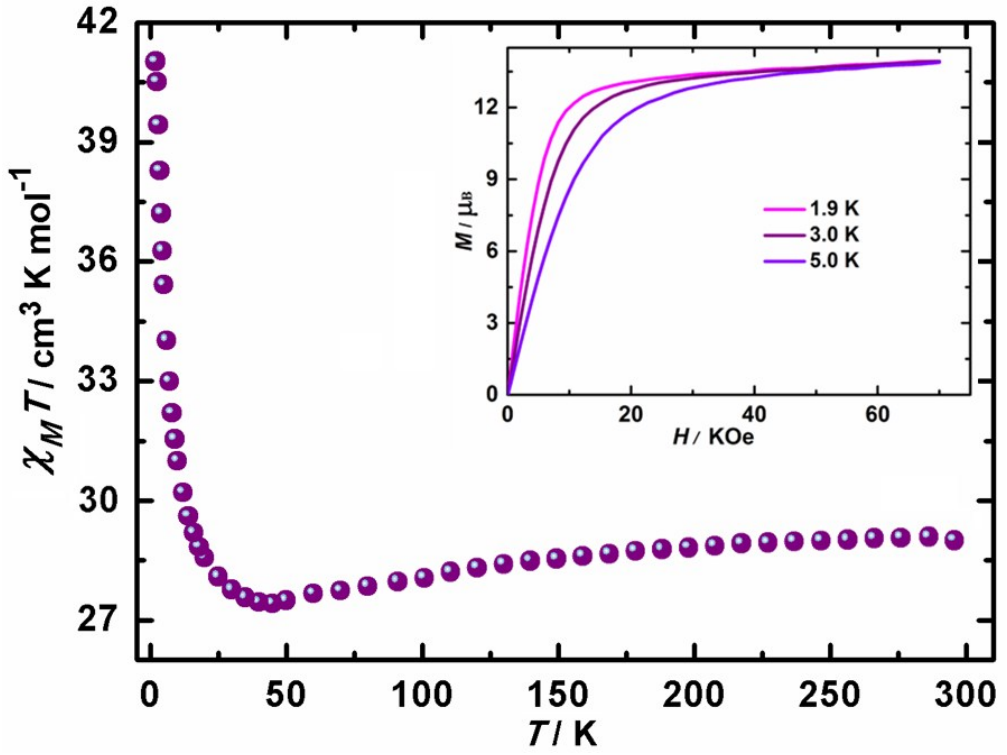

Figure S8. Temperature dependence of the $\chi_M T$ product at 1 kOe for **1a**; inset: *M vs. H/T* plot at different temperatures below 5 K.

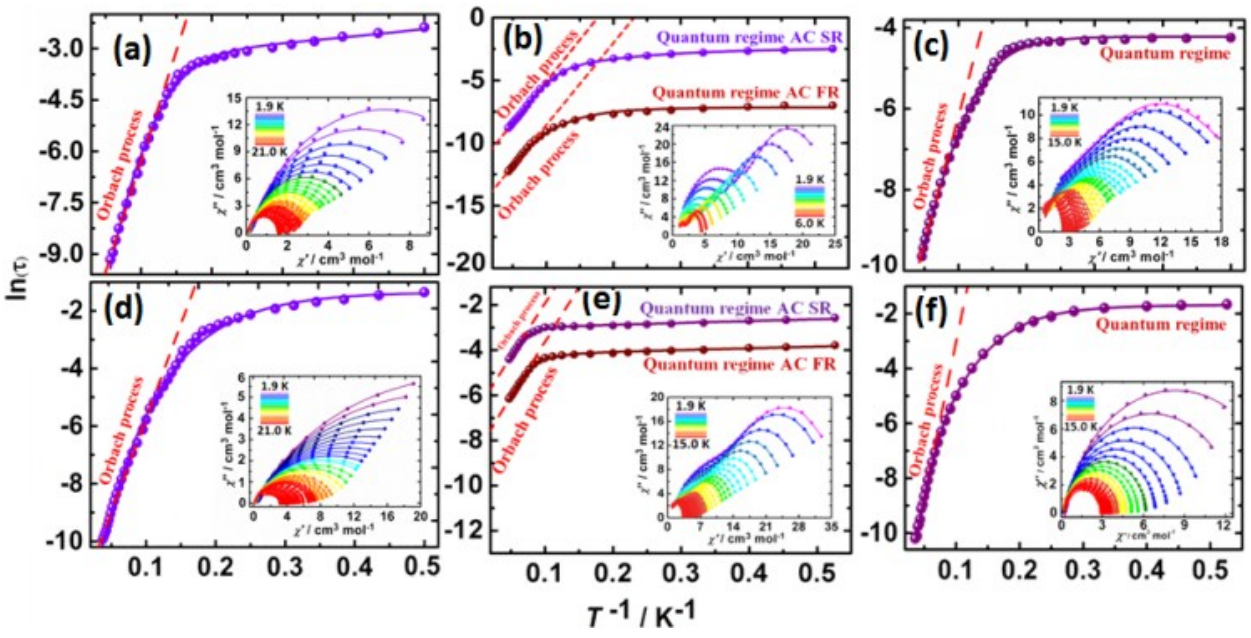

Figure 9. Magnetization relaxation time, lnτ, versus T^{-1} plots under zero-dc field and Argand plots (inset) for **1** (a), **2** (b), **1a** (c) and diluted ($Dy_{0.1}Y_{0.9}$) sample of **2** (d). The solid lines represent the best fits.

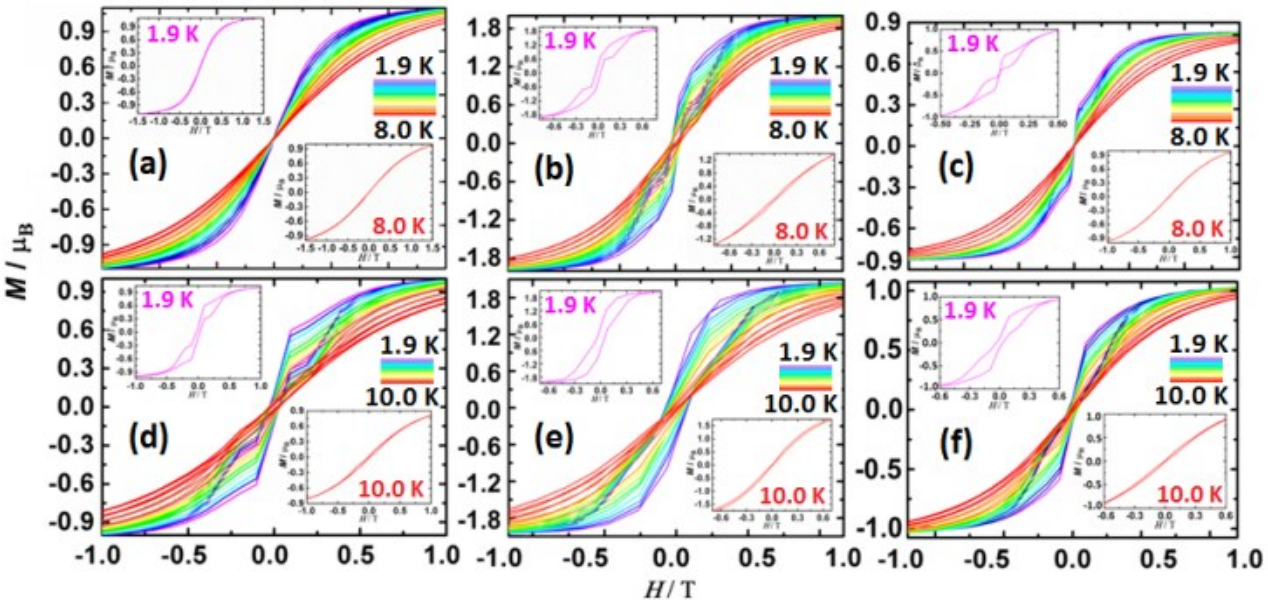

Figure 10. Magnetic hysteresis for **1** (a), **2** (b), **1a** (c) and diluted ($Dy_{0.1}Y_{0.9}$) sample of **1** (d), **2** (e), **1a** (f) with clear opening of the hysteresis loop under a constant field sweep rate of 0.02 Ts^{-1}.

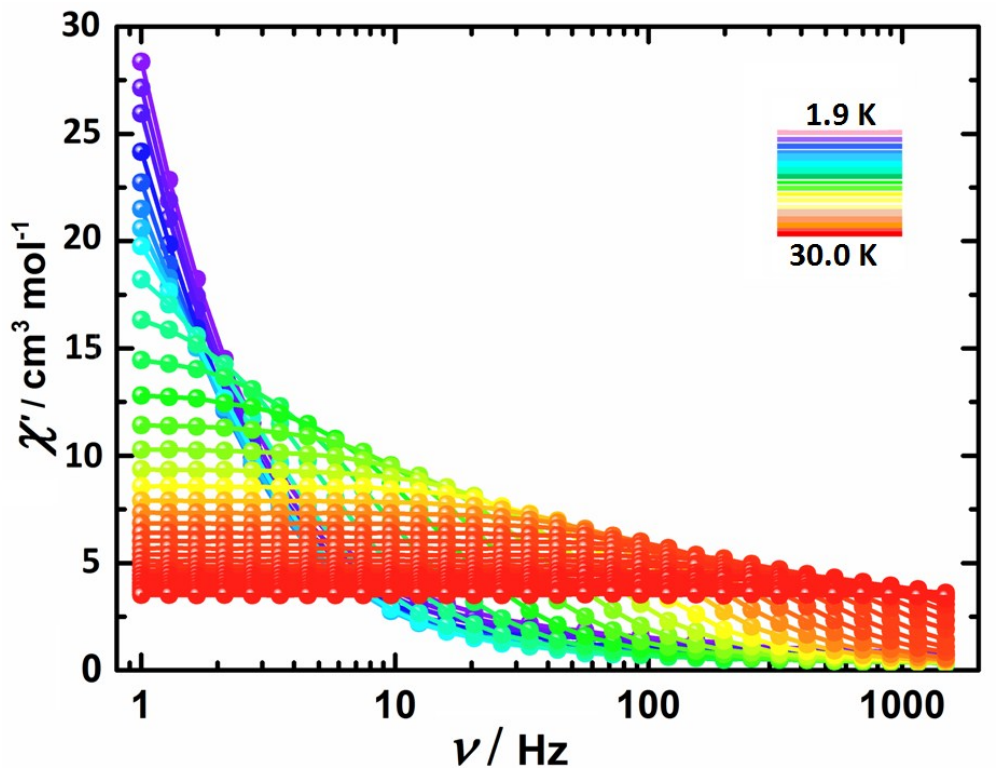

Figure S11. Frequency dependence of the χ' product, *ac* susceptibility under zero dc field for compound **1**.

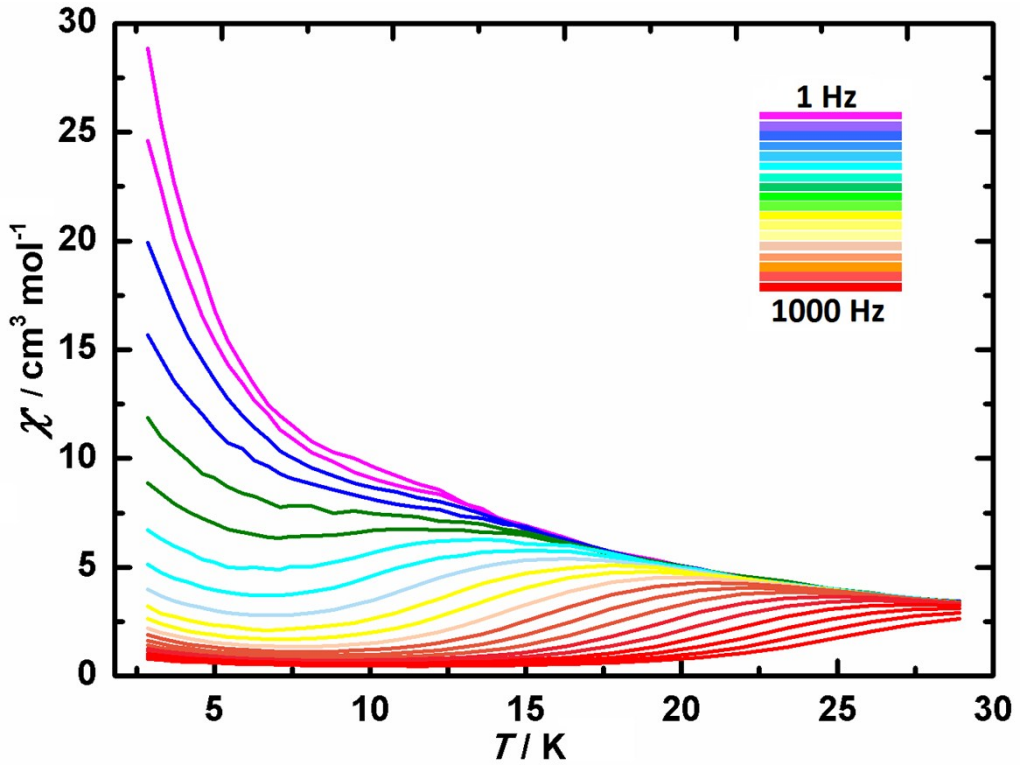

Figure S12. Temperature dependence of the χ' product, *ac* susceptibility under zero-dc field for **1**.

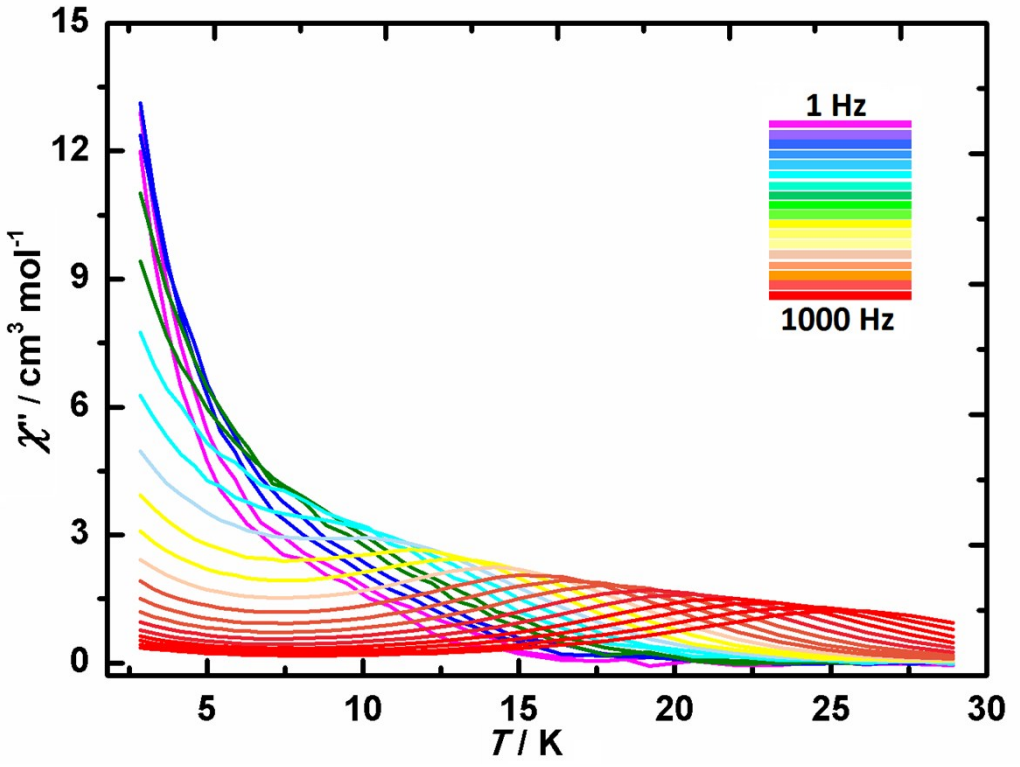

Figure S13. Temperature dependence of the χ'' product, *ac* susceptibility under zero-dc field for compound **1**.

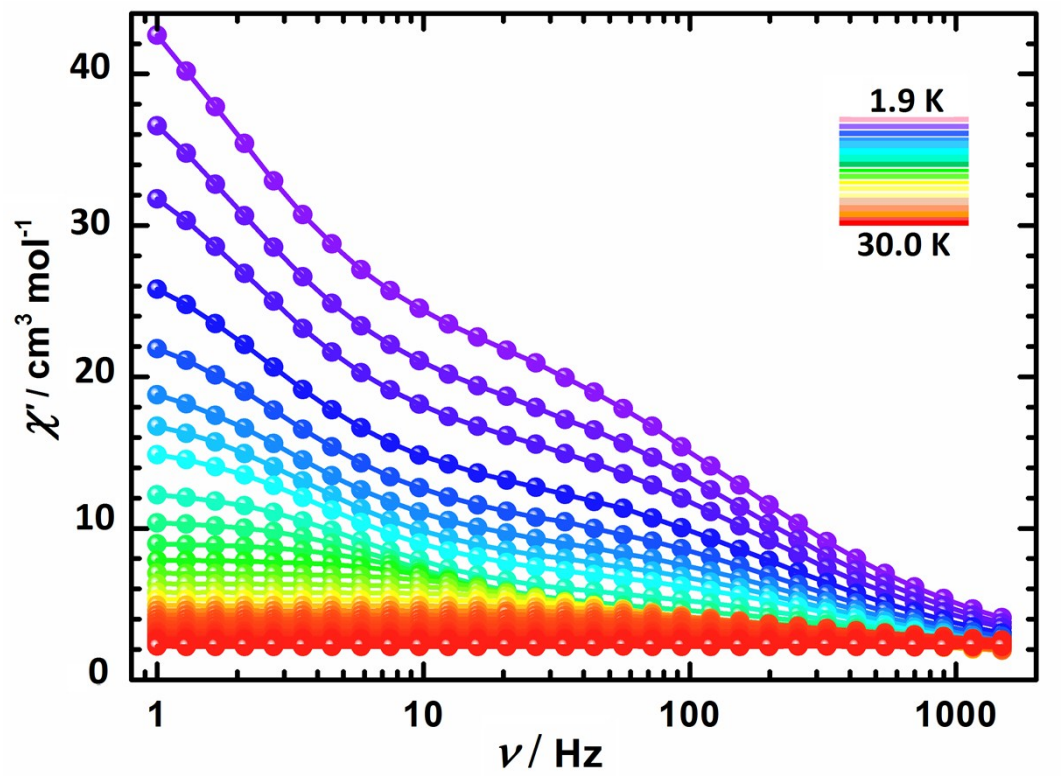

Figure S14. Frequency dependence of the χ' product, *ac* susceptibility under zero dc field for compound **2**.

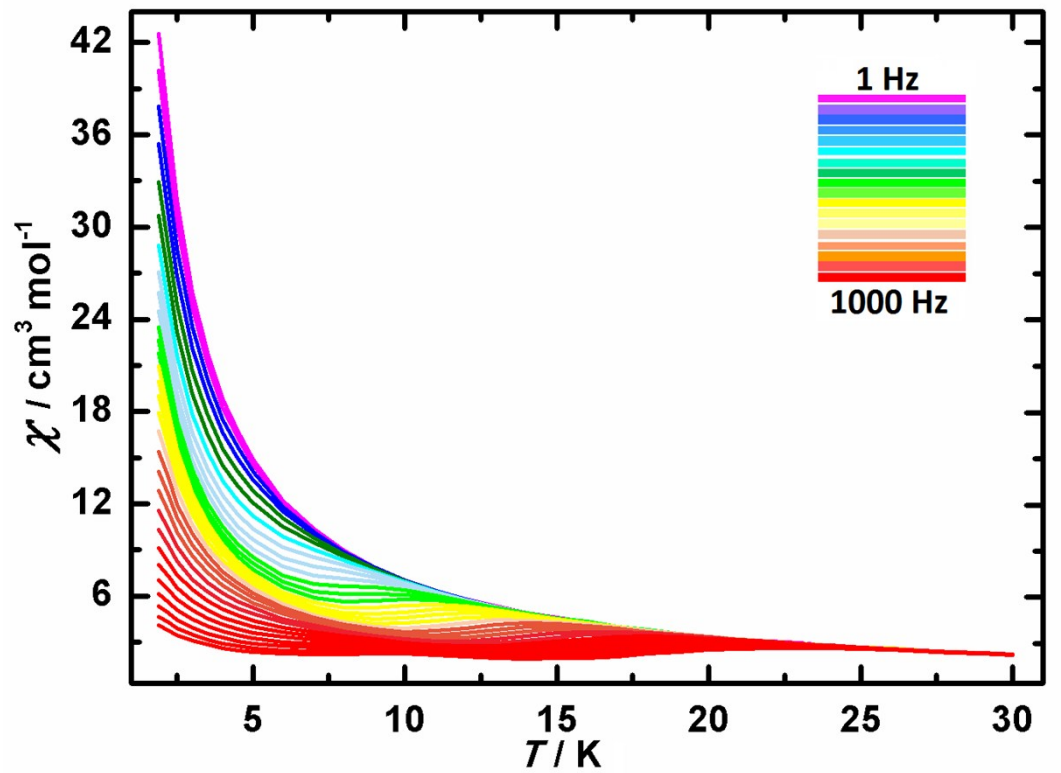

Figure S15. Temperature dependence of the χ' product, *ac* susceptibility under zero-dc field for **2**.

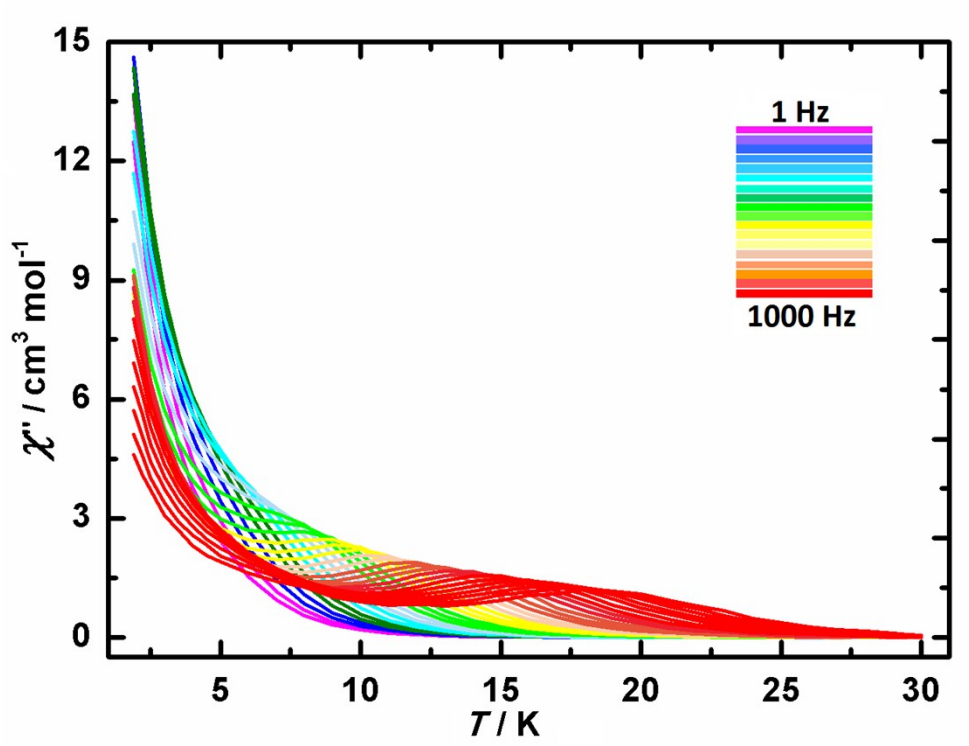

Figure S16. Temperature dependence of the χ'' product, *ac* susceptibility under zero-dc field for compound **2**.

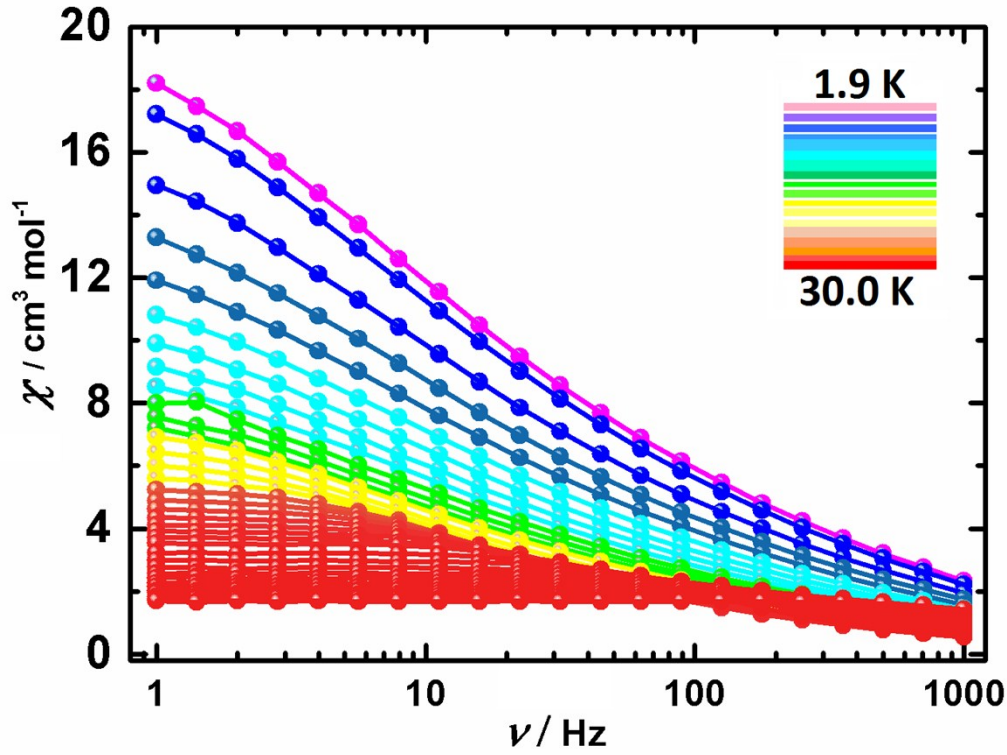

Figure S17. Frequency dependence of the χ' product, *ac* susceptibility under zero dc field for compound **1a**.

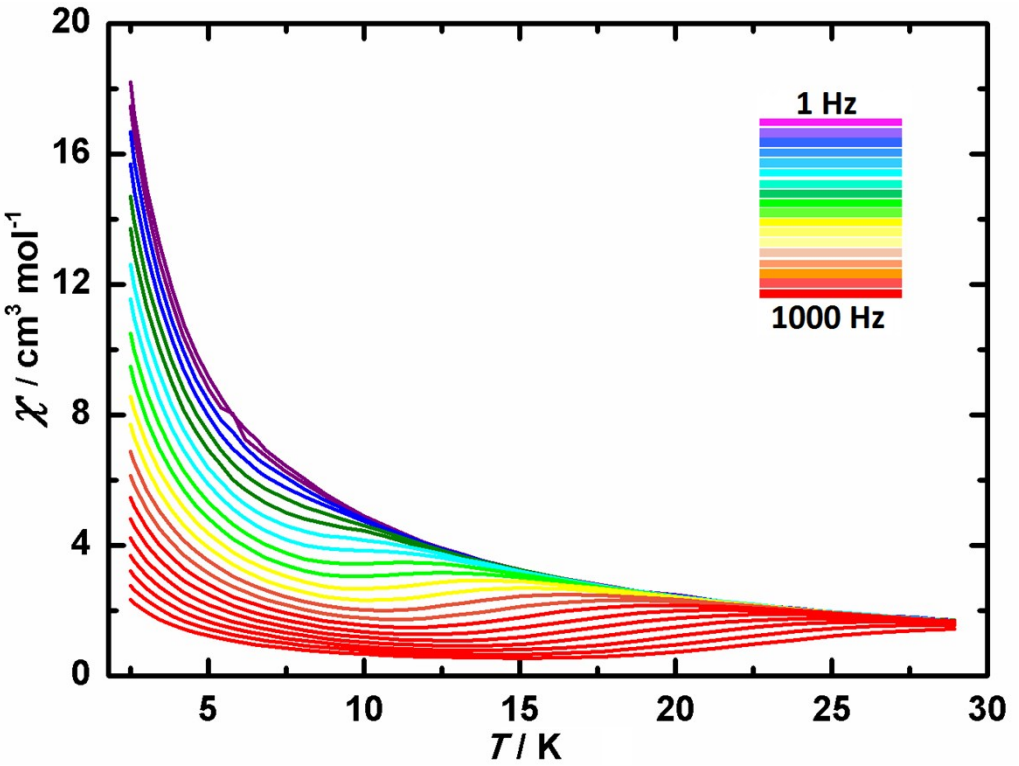

Figure S18. Temperature dependence of the χ' product, *ac* susceptibility under zero-dc field for **1a**.

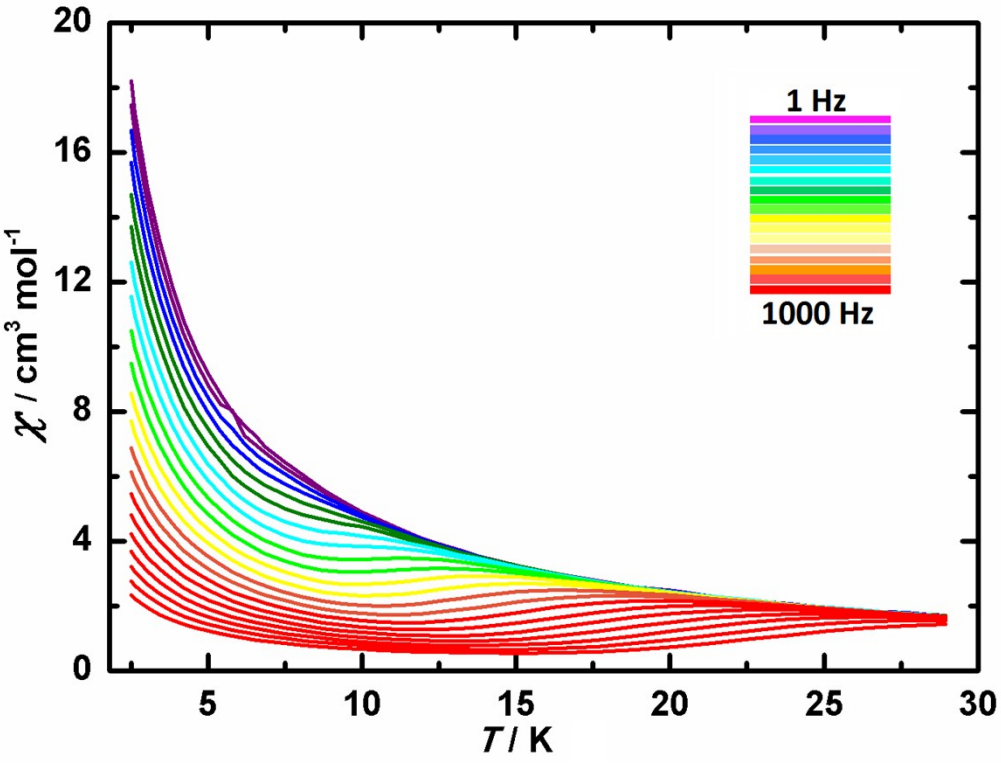

Figure S19. Temperature dependence of the χ'' product, *ac* susceptibility under zero-dc field for compound **1a**.

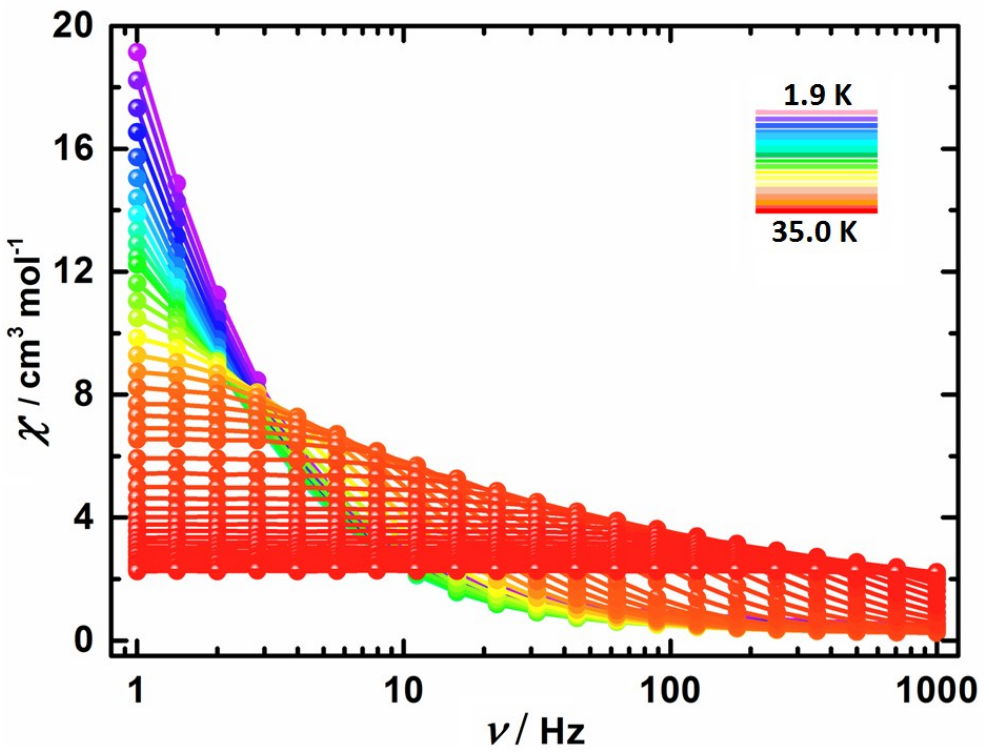

Figure S20. Frequency dependence of the χ' product, *ac* susceptibility under zero dc field for diluted sample of **1** ($Dy_{0.1}Y_{0.9}$).

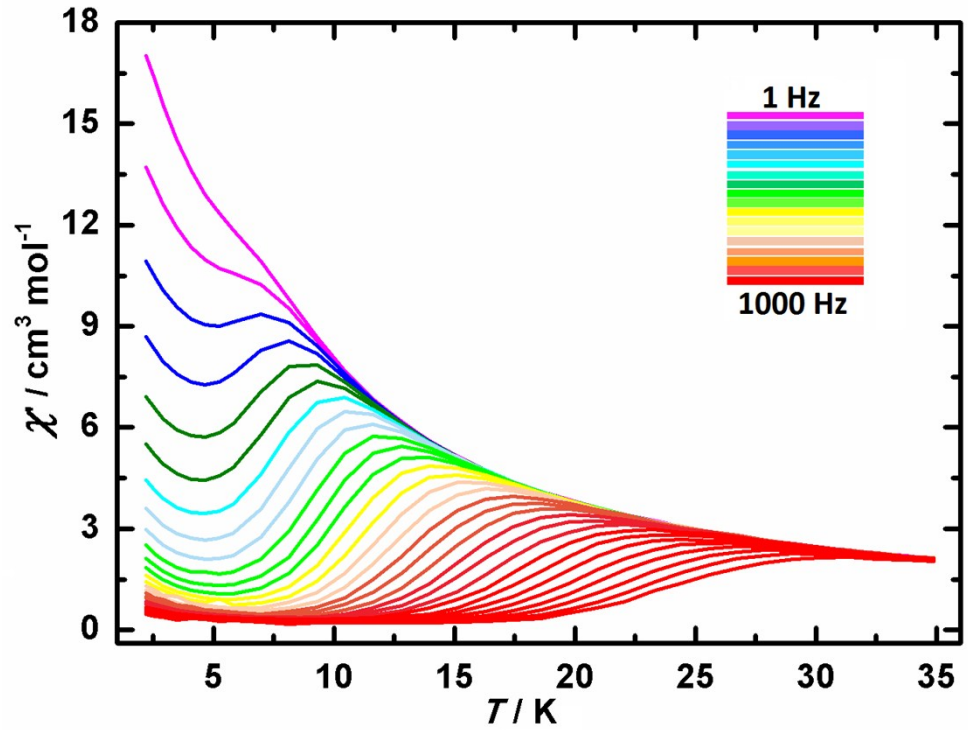

Figure S21. Temperature dependence of the χ' product, *ac* susceptibility under zero-dc field for diluted sample of **1** ($Dy_{0.1}Y_{0.9}$).

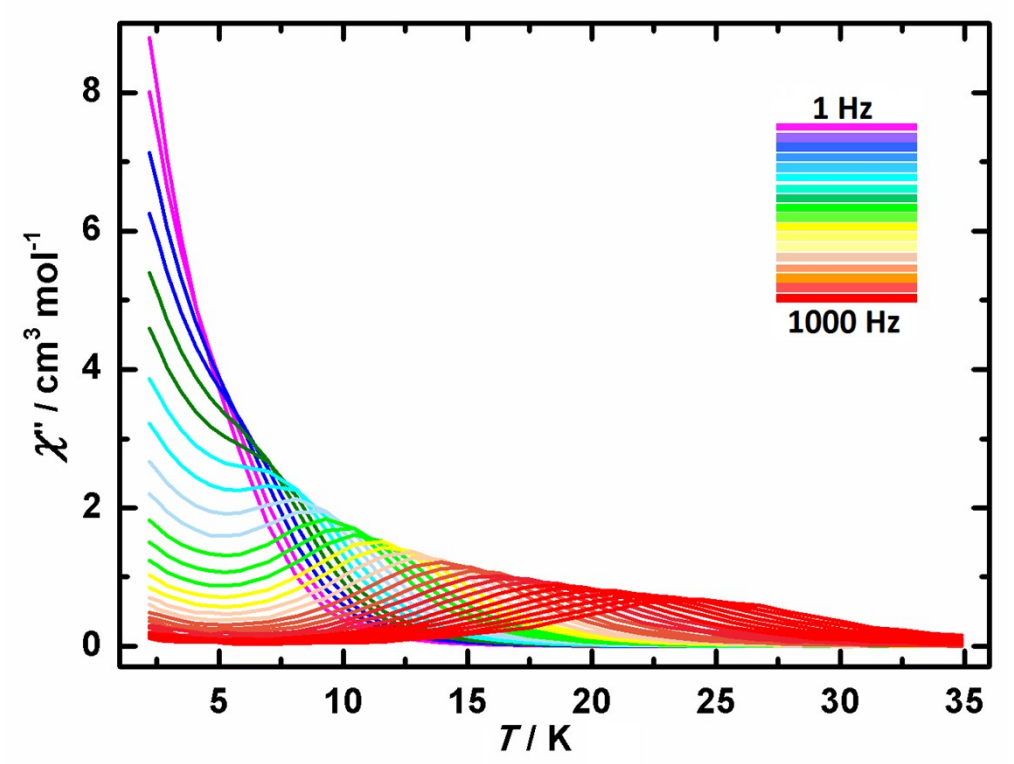

Figure S22. Temperature dependence of the χ'' product, *ac* susceptibility under zero-dc field for diluted sample of **1** ($Dy_{0.1}Y_{0.9}$).

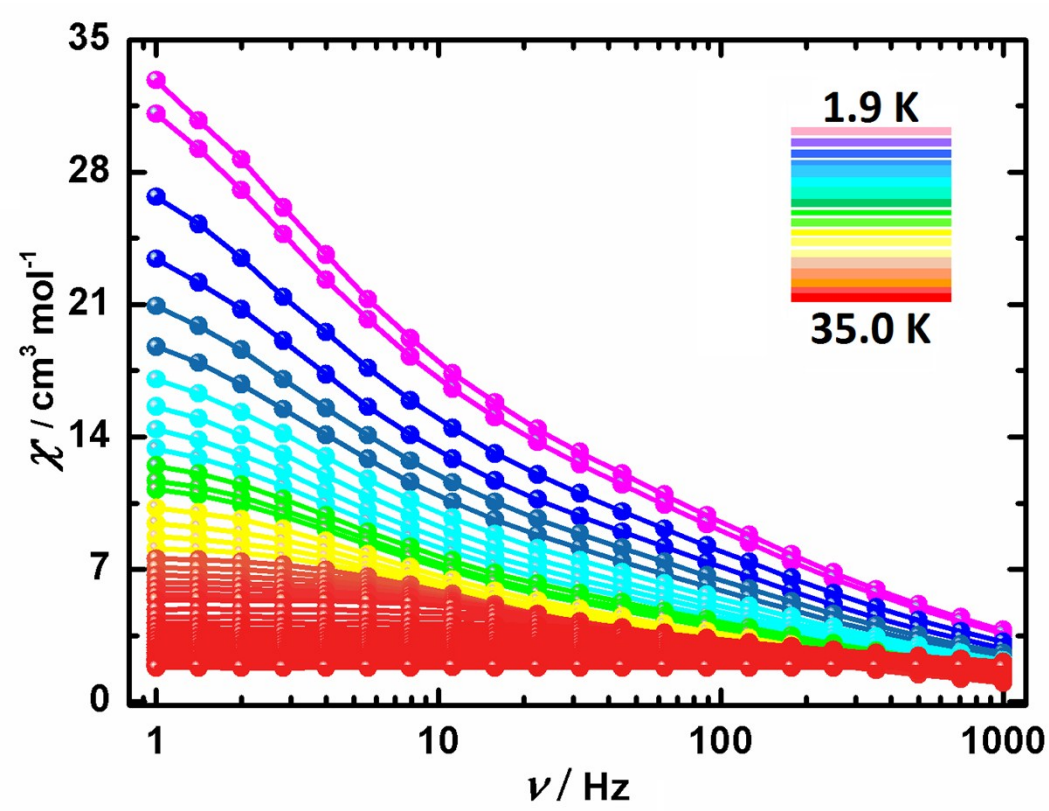

Figure S23. Frequency dependence of the χ' product, *ac* susceptibility under zero dc field for diluted sample of **2** ($Dy_{0.1}Y_{0.9}$).

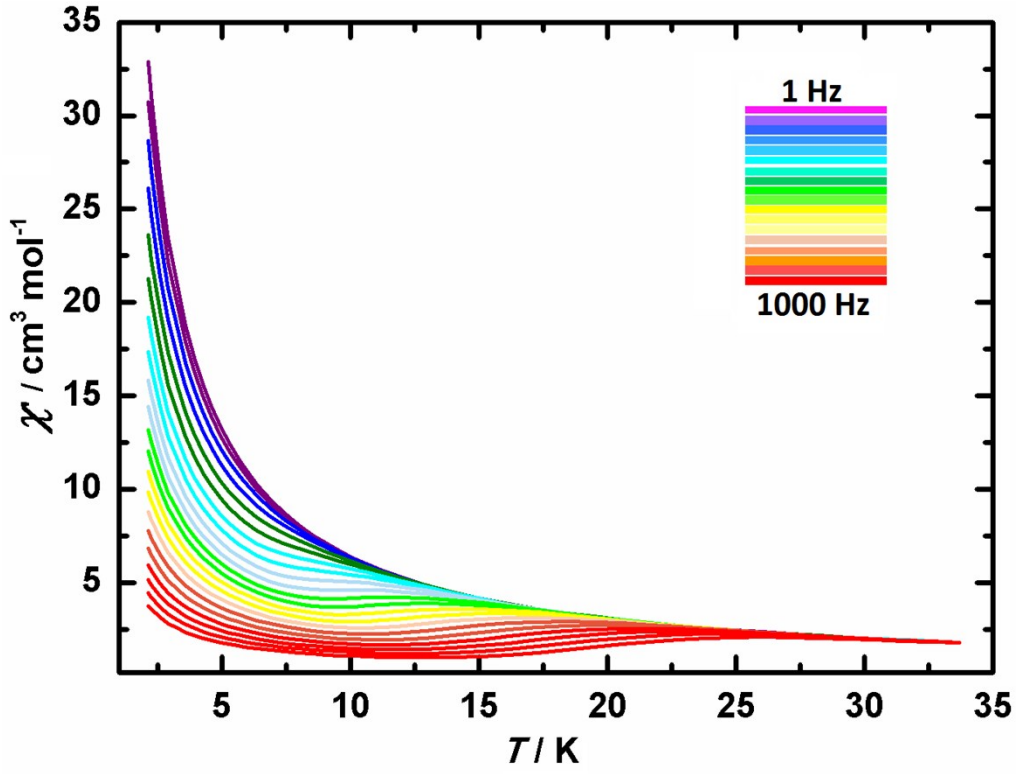

Figure S24. Temperature dependence of the χ' product, *ac* susceptibility under zero-dc field for diluted sample of **2** ($Dy_{0.1}Y_{0.9}$).

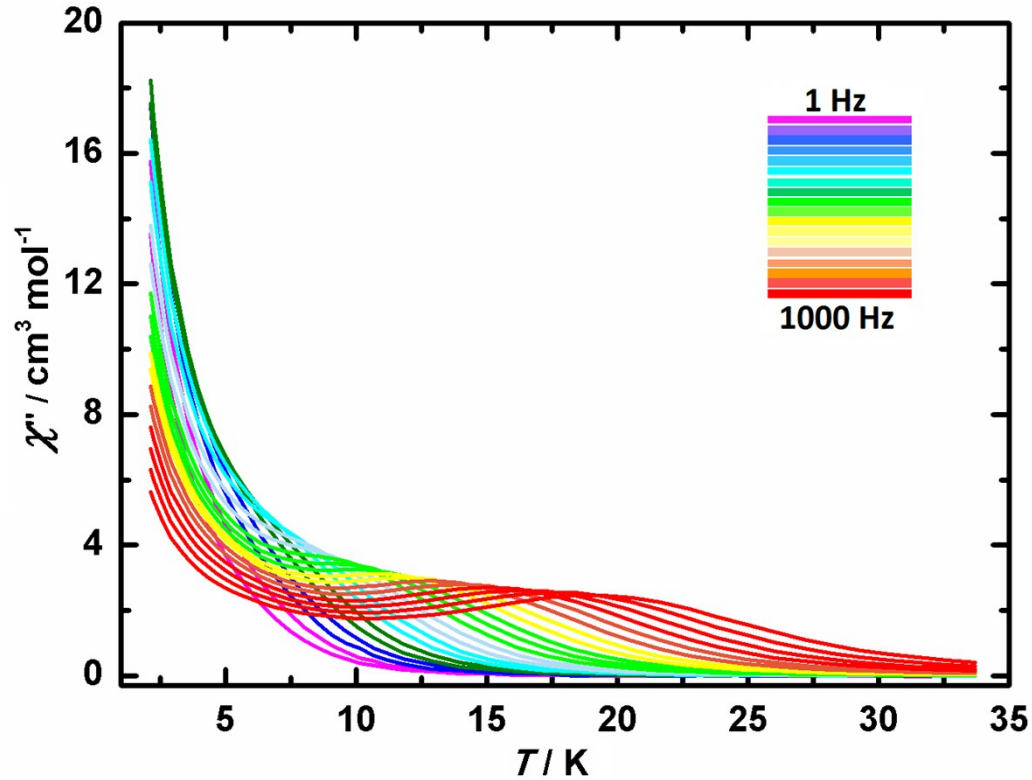

Figure S25. Temperature dependence of the χ'' product, *ac* susceptibility under zero-dc field for diluted sample of **2** ($Dy_{0.1}Y_{0.9}$).

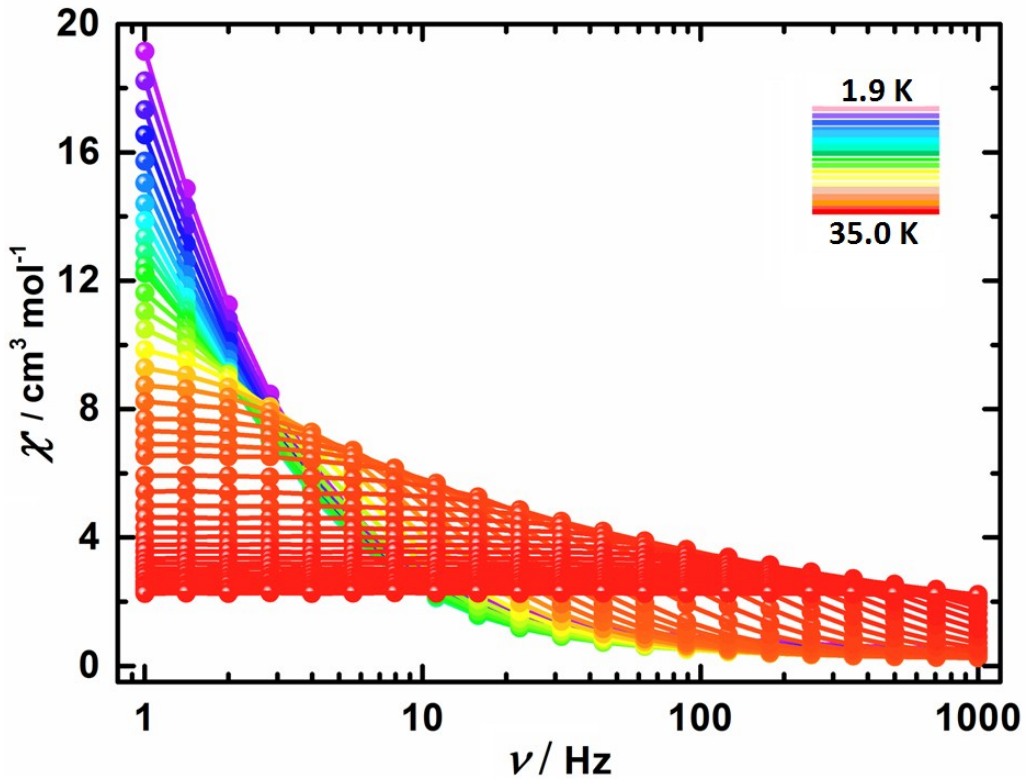

Figure S26. Frequency dependence of the χ' product, *ac* susceptibility under zero dc field for diluted sample of **1a** ($Dy_{0.1}Y_{0.9}$).

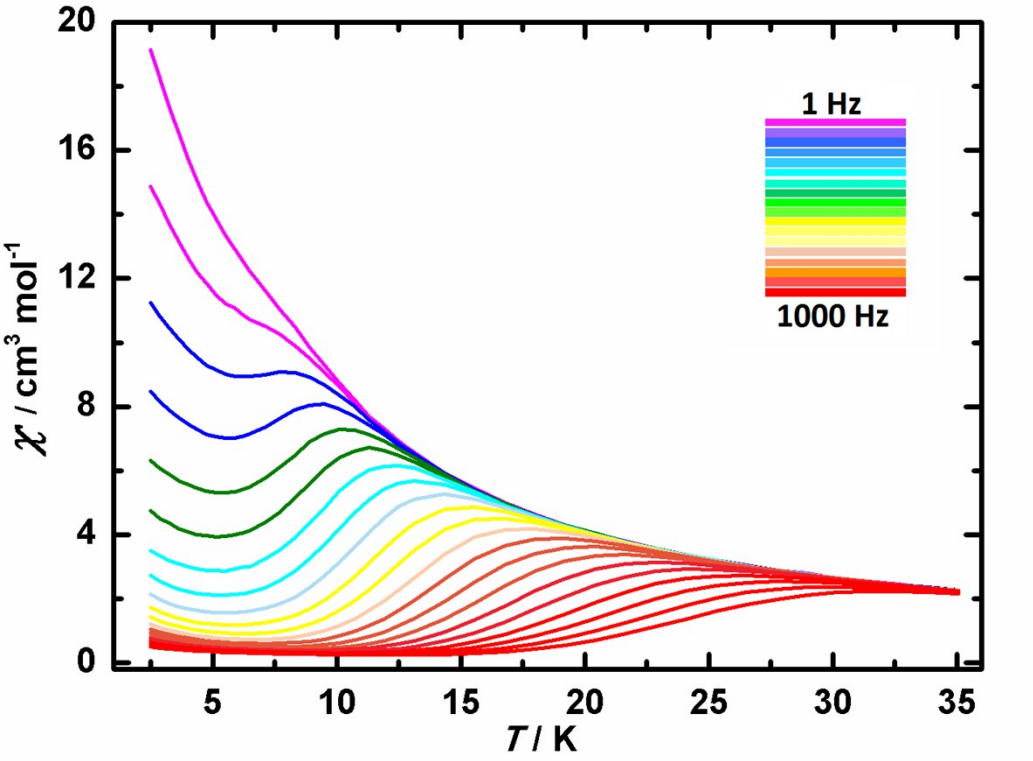

Figure S27. Temperature dependence of the χ' product, *ac* susceptibility under zero-dc field for diluted sample of **1a** ($Dy_{0.1}Y_{0.9}$).

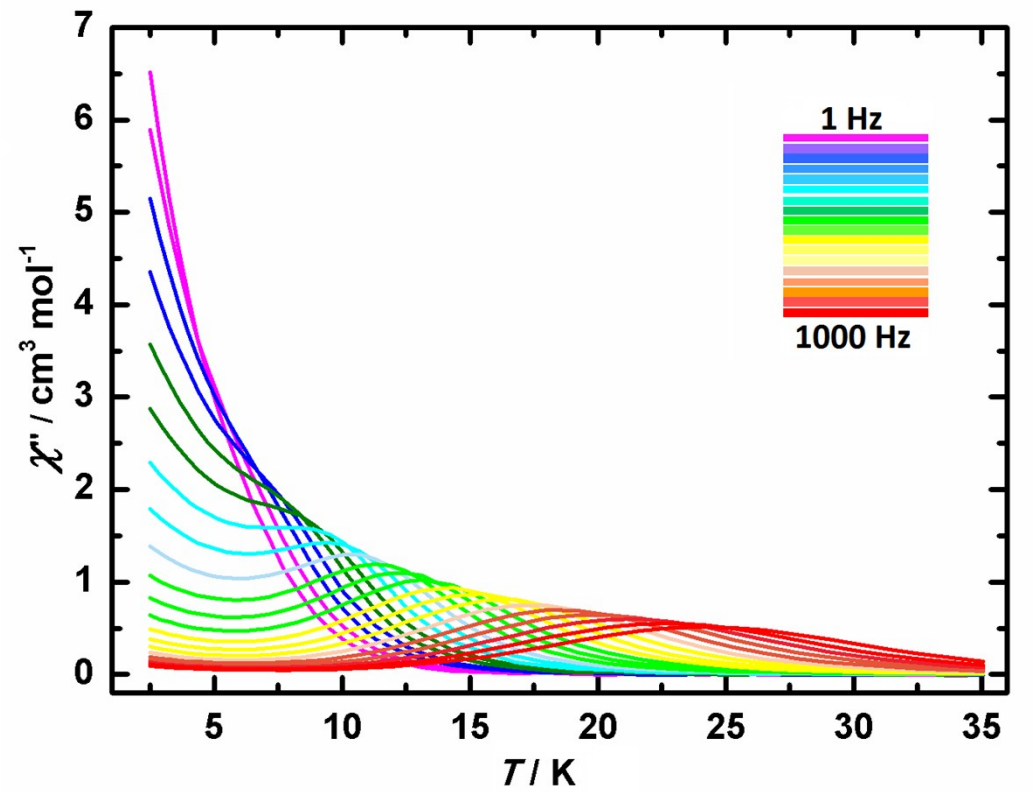

Figure S28. Temperature dependence of the χ'' product, *ac* susceptibility under zero-dc field for diluted sample of **1a** ($Dy_{0.1}Y_{0.9}$).

Computational details

Binuclear complexes **1**, **1a-I** and **1a-II** have an inversion center, and thus only one individual Dy^{III} fragment for each was calculated. The double chloride-bridged compound **2** has two types of individual Dy^{III} fragments to be calculated. Complete-active-space self-consistent field (CASSCF) calculations on individual Dy^{III} fragments (see Figure S1 for the calculated model structures of **1**, **1a-I**, **1a-II**, **2-Dy1** and **2-Dy2** extracted from the compounds **1**, **1a** and **2** on the basis of single-crystal X-ray determined geometry have been carried out with MOLCAS 8.2 program package.[5] For **1**, **1a-I**, **1a-II**, **2-Dy1** and **2-Dy2**, each individual Dy^{III} fragment was calculated keeping the experimentally determined structure of the corresponding compound while replacing the other Dy^{III} ions by diamagnetic Lu^{III}.

The basis sets for all atoms are atomic natural orbitals from the MOLCAS ANO-RCC library: ANO-RCC-VTZP for Dy^{III} ion; VTZ for close O or N; VDZ for distant atoms. The calculations employed the second order Douglas-Kroll-Hess Hamiltonian, where scalar relativistic contractions were taken into account in the basis set and the spin-orbit couplings were handled separately in the restricted active space state interaction (RASSI-SO) procedure. For individual Dy^{III} fragments, active electrons in 7 active spaces include all *f* electrons (CAS(9 in 7)) in the CASSCF calculation. To exclude all the doubts, we calculated all the roots in the active space. We have mixed the maximum number of spin-free state which was possible with our hardware (all from 21 sextets, 128 from 224 quadruplets, 130 from 490 doublets). Single_Aniso[6] program was used to obtain the energy levels, *g* tensors, m_J values, magnetic axes, *et al.,* based on the above CASSCF/RASSI calculations.

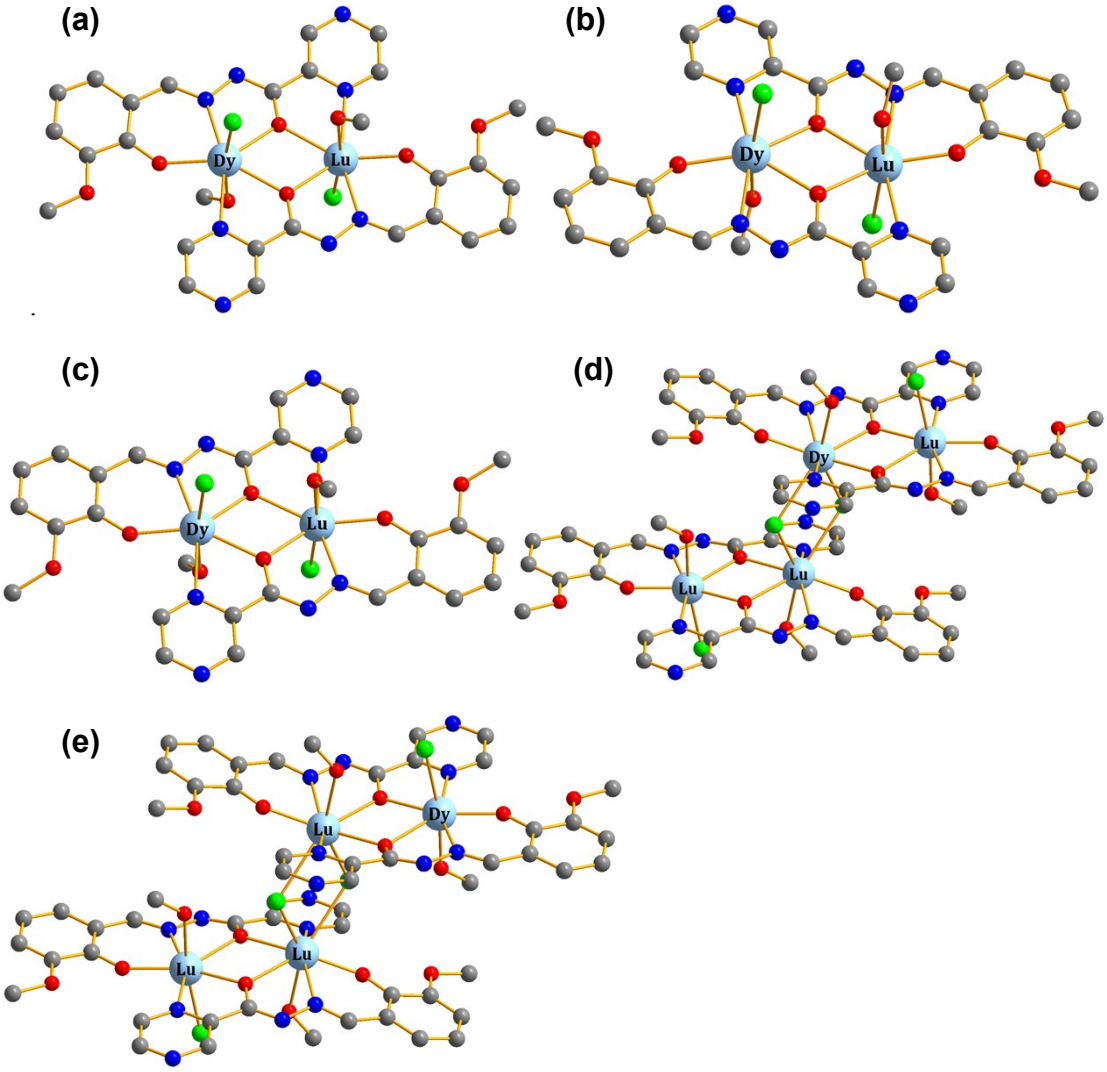

Figure S29. Calculated model structures of individual Dy^{III} fragments of **1** (a), **1a-I** (b), **1a-II** (c), **2-Dy1** (d) and **2-Dy2** (e); H atoms are omitted.

Table S10. Calculated energy levels (cm^{-1}), ***g*** (g_x, g_y, g_z) tensors and m_J values of the lowest eight Kramers doublets (KDs) of individual Dy^{III} fragments of **1**, **1a-I**, **1a-II**, **2-Dy1** and **2-Dy2** using CASSCF/RASSI with MOLCAS 8.2.

KDs	**1**			**1a-I**			**1a-II**		
	E/cm^{-1}	g	m_J	E/cm^{-1}	***g***	m_J	E/cm^{-1}	g	m_J
1	0.0	0.014 0.025 19.613	±15/2	0.0	0.006 0.011 19.736	±15/2	0.0	0.014 0.024 19.717	±15/2
2	196.1	0.204 0.250 16.816	±13/2	224.0	0.132 0.172 17.028	±13/2	270.4	0.333 0.547 16.457	±13/2
3	384.2	2.184 3.480 12.440	±11/2	411.4	1.906 2.298 12.887	±11/2	485.4	3.170 5.767 10.665	±11/2
4	448.5	10.998	±5/2	484.9	2.975	±7/2	618.8	7.683	±9/2

		7.140 2.259			5.982 11.959			5.613 1.038	
5	507.5	1.889 5.036 11.007	±3/2	534.5	11.631 6.178 0.589	±5/2	799.3	1.937 2.482 11.368	±7/2
6	580.0	2.612 4.591 11.433	±7/2	599.4	2.637 4.558 10.693	±9/2	982.5	0.481 0.656 14.765	±3/2
7	653.8	0.478 3.359 13.953	±1/2	658.5	1.528 1.931 16.963	±3/2	1177.0	0.028 0.030 17.286	±1/2
8	692.8	0.665 2.762 16.472	±9/2	723.6	0.203 0.333 19.154	±1/2	1412.9	0.003 0.004 19.812	±5/2
KDs	**2-Dy1**			**2-Dy2**					
	E/cm^{-1}	g	m_J	E/cm^{-1}	g	m_J			
1	0.0	0.004 0.006 19.722	±15/2	0.0	0.007 0.012 19.664	±15/2			
2	182.7	0.107 0.154 16.949	±13/2	235.2	0.121 0.155 16.861	±13/2			
3	329.2	2.645 5.732 12.603	±11/2	457.9	1.607 2.546 12.793	±11/2			
4	372.5	3.417 4.950 8.631	±9/2	563.7	9.766 7.211 3.515	±9/2			
5	462.5	9.700 6.805 3.838	±7/2	629.3	0.830 1.700 15.644	±1/2			
6	526.9	1.214 3.927 10.889	±3/2	687.3	0.036 2.893 11.841	±7/2			
7	554.5	0.235 1.772 13.236	±1/2	750.5	1.579 2.476 16.880	±5/2			
8	623.8	0.077 0.193 19.491	±5/2	824.4	0.086 0.106 19.043	±3/2			

Table S11. Wave functions with definite projection of the total moment | m_J > for the lowest two Kramers doublets (KDs) of individual Dy^{III} fragments of **1**, **1a-I**, **1a-II**, **2-Dy1** and **2-Dy2** using CASSCF/RASSI with MOLCAS 8.2.

	E/cm^{-1}	wave functions
1	0.0	95%|±15/2>
	196.1	88%|±13/2>+4%|±11/2>+5%|±9/2>
1a-I	0.0	98%|±15/2>
	224.0	86%|±13/2>+6%|±11/2>+4%|±9/2>
1a-II	0.0	97%|±15/2>
	270.4	83%|±13/2>+10%|±9/2>
2-Dy1	0.0	97%|±15/2>
	182.7	88%|±13/2>+4%|±11/2>+4%|±9/2>
2-Dy2	0.0	96%|±15/2>
	235.2	88%|±13/2>+3%|±11/2>+6%|±9/2>

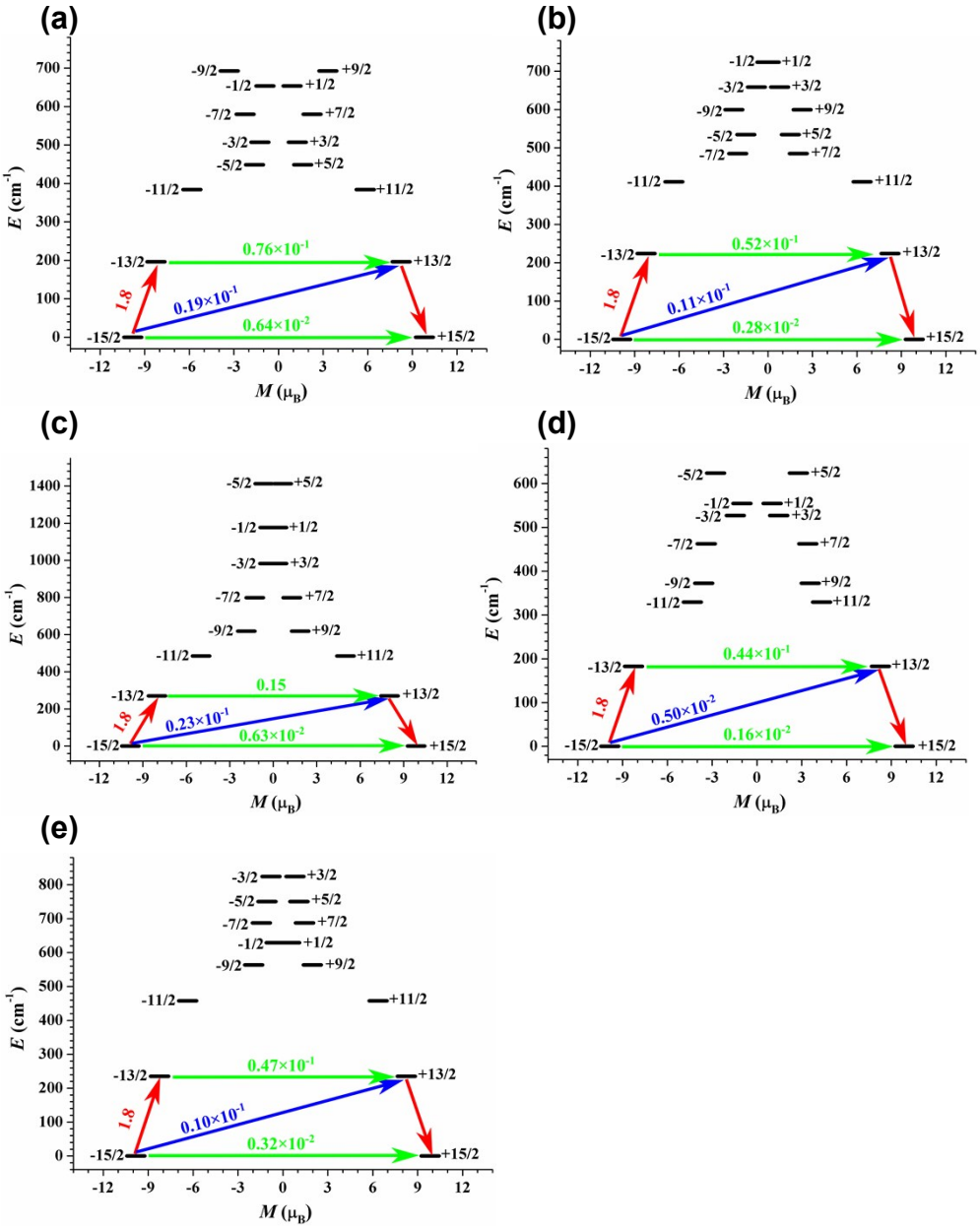

Figure S30. Magnetization blocking barriers for individual Dy^{III} fragments of **1** (a), **1a-I** (b), **1a-II** (c), **2-Dy1** (d) and **2-Dy2** (e). The thick black lines represent the Kramers doublets as a function of their magnetic moment along the magnetic axis. The green lines correspond to the diagonal matrix element of the transversal magnetic moment; the blue lines represent Orbach relaxation processes. The path shown by the red arrows represents the most probable path for magnetic relaxation in the corresponding compounds. The numbers at each arrow stand for the mean absolute value of the corresponding matrix element of transition magnetic moment.

To fit the exchange interactions in **1**, **1a-I**, **1a-II** and **2**, we took two steps to obtain them. Firstly, we calculated individual Dy^{III} fragments using CASSCF to obtain the corresponding magnetic properties. Then, the exchange interaction between the magnetic centers is considered within the Lines model,[7] while the account of the dipole-dipole magnetic coupling is treated exactly. The Lines model is effective and has been successfully used widely in the research field of *f*-element single-molecule magnets.[8] For **1**, **1a-I** and **1a-II**, there is only one type of *J*. The exchange Ising Hamiltonian is:

$$\hat{H}_{exch} = -J \hat{S}_{Dy1} \hat{S}_{Dy2} \quad \text{(S1)}$$

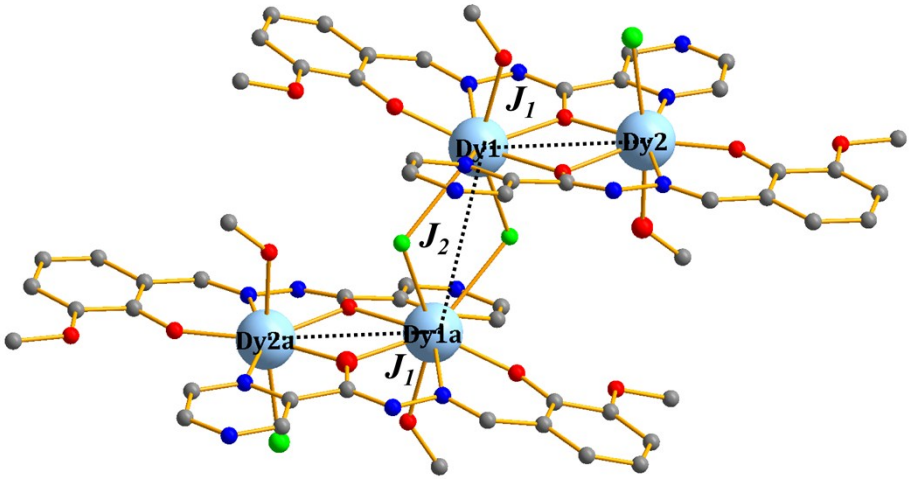

Figure S31. Two types of J_1 and J_2 in complex **2**.

For **2**, we only considered three types of *J* shown in Figure S3. The exchange Ising Hamiltonian is:

$$\hat{H}_{exch} = -J_1(\hat{S}_{Dy1} \hat{S}_{Dy2} + \hat{S}_{Dy1a} \hat{S}_{Dy2a}) - J_2 \hat{S}_{Dy1} \hat{S}_{Dy1a} \quad \text{(S2)}$$

The total J is the parameter of the total magnetic interaction ($J = J_{diploar} + J_{exchange}$) between Dy^{III} ions. The $\tilde{S}_{Dy} = \pm 1/2$ is the ground pseudospin on the Dy^{III} sites. The dipolar magnetic coupling can be calculated exactly, while the exchange coupling constants were fitted through comparison of the computed and measured magnetic susceptibilities using the Poly_Aniso program.[6]

Table S12. Exchange energies (cm^{-1}) and main values of the g_z for the lowest two or eight exchange

doublets of **1**, **1a-I**, **1a-II** and **2**.

	1		**1a-I**		**1a-II**		**2**	
	E/cm^{-1}	g_z	E/cm^{-1}	g_z	E/cm^{-1}	g_z	E/cm^{-1}	g_z
1	0.0	39.228	0.0	39.474	0.0	39.435	0.0	78.152
2	1.2	0.000	4.0	0.000	4.2	0.000	0.7	0.000
3							2.4	0.144
4							2.4	0.144
5							2.6	39.332
6							2.6	39.332
7							4.6	0.000
8							4.8	9.896

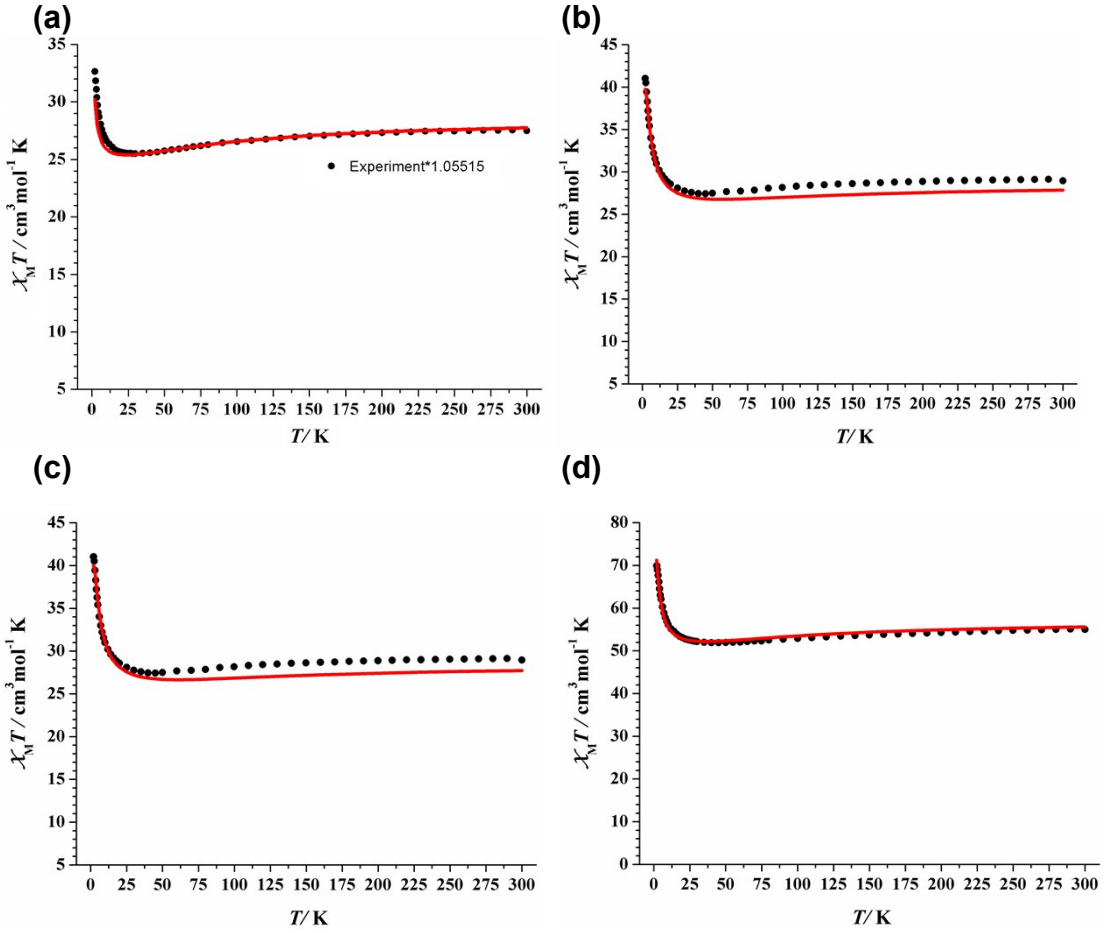

Figure S32. Calculated (red solid line) and experimental (black circle dot) data of magnetic susceptibilities of **1** (a), **1a-I** (b), **1a-II** (c) and **2** (d). The intermolecular interactions zJ' of these compounds were fitted to −0.01, −0.01, −0.01 and −0.005 cm^{-1}, respectively.

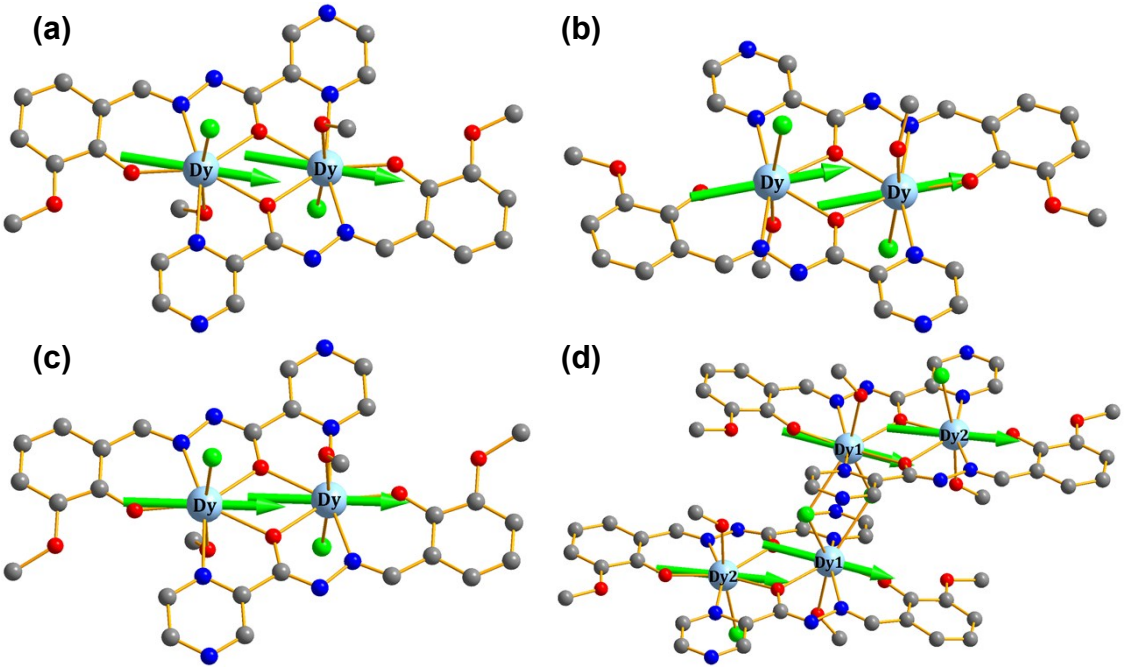

Figure S33. Calculated orientation of the local main magnetic axes of the ground Kramers doublet on Dy^{III} ions of **1** (a), **1a-I** (b), **1a-II** (c) and **2** (d).

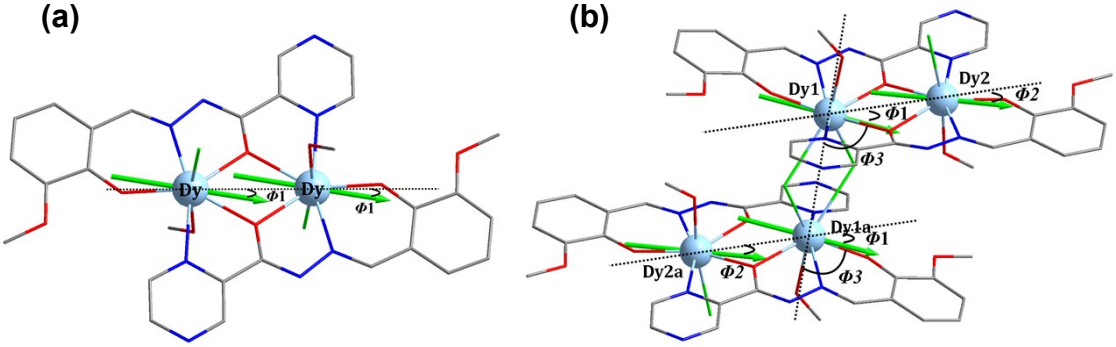

Figure S34. Label of the angle Φ between the main magnetic axis with the unit vector connecting two Dy^{III} sites for **1** (a) and **2** (b).

Table S13. Angle Φ between the main magnetic axis with the unit vector connecting two Dy^{III} sites for **1**, **1a-I**, **1a-II** and **2**.

angle	**1**	**1a_I**	**1a_II**	**2**
Φ1	21.2 °	14.6 °	14.6 °	22.0 °
Φ2				16.5 °
Φ3				74.5 °

References:

5. (a) F. Aquilante, L. De Vico, N. Ferré, G. Ghigo, P.-Å. Malmqvist, P. Neogrády, T. B. Pedersen, M. Pitonak, M. Reiher, B. O. Roos, L. Serrano-Andrés, M. Urban, V. Veryazov, R. Lindh, *J. Comput. Chem.*, 2010, **31**, 224-247; (b) V. Veryazov, P. -O. Widmark, L. Serrano-Andres, R. Lindh, B. O. Roos, *Int. J. Quantum Chem.*, 2004, **100**, 626-635; (c) G. Karlström, R. Lindh, P. -Å. Malmqvist, B. O. Roos, U. Ryde, V. Veryazov, P.-O. Widmark, M. Cossi, B. Schimmelpfennig, P. Neogr´ady, L. Seijo, *Comput. Mater. Sci.*, 2003, **28**, 222-239.
6. (a) L. F. Chibotaru, L. Ungur, A. Soncini, Angew. Chem. Int. Ed., 2008, **47**, 4126-4129; (b) L. Ungur, W. Van den Heuvel, L. F. Chibotaru, New J. Chem., 2009, **33**, 1224-1230; (c) L. F. Chibotaru, L. Ungur, C. Aronica, H. Elmoll, G. Pilet, D. Luneau, *J. Am. Chem. Soc.*, 2008, **130**, 12445-12455.
7. M. E. Lines, *J. Chem. Phys.*, 1971, **55**, 2977-2984.
8. (a) K. C. Mondal, A. Sundt, Y. H. Lan, G. E. Kostakis, O. Waldmann, L. Ungur, L. F. Chibotaru, C. E. Anson, A. K. Powell, *Angew. Chem. Int. Ed.*, 2012, **51**, 7550-7554; (b) S. K. Langley, D. P. Wielechowski, V. Vieru, N. F. Chilton, B. Moubaraki, B. F. Abrahams, L. F. Chibotaru, K. S. Murray, *Angew. Chem. Int. Ed.*, 2013, **52**, 12014-12019.